2004

Tissue interactions with lasers and liquid nitrogen: a novel cryopreservation method

Deepak Kandra
Louisiana State University and Agricultural and Mechanical College, dkandr1@lsu.edu

TISSUE INTERACTIONS WITH LASERS AND LIQUID NITROGEN – A NOVEL CRYOPRESERVATION METHOD

A Thesis

Submitted to the Graduate Faculty of the
Louisiana State University and
Agricultural and Mechanical College
In partial fulfillment of the
requirements for the degree of
Master of Science in Mechanical Engineering

in

The Department of Mechanical Engineering

by

Deepak Kandra
B.E, Bangalore University, 2001
December 2004

Acknowledgements

It has been a pleasure to be guided, motivated and supported by the two most wonderful people I have ever met, Dr. Ram V. Devireddy and Dr. Tryfon T. Charalampopoulos, and to whom I dedicate this thesis. I would like to thank my advisor Dr. Ram V. Devireddy for introducing me to the field of Biotechnology, by giving me a chance to work on such an intriguing problem and for the technical insight he has provided. I would like to thank my co-advisor Dr. Tryfon T. Charalampopoulos for inculcating in me the morals of research and always encouraging me to work hard as a graduate student. Next I would like to thank Dr. Michael C. Murphy for being my committee member and for his time and expertise to evaluate my thesis.

Special thanks to Dr. Mayank Tyagi, Dr. Kumar V. Singh, Dr. Keith A. Gonthier and Dr. Dorel Moldovan for the fruitful discussions I had with them on interface tracking and front capturing techniques. Then I would like to thank Kellie N. Huckaby for helping me out in the experiments and for patiently taking the pictures of the vitrified samples. I would also like to acknowledge Dr. J. Gimble at the Pennington Biomedical Research Center for providing me with the adipose tissue derived adult stem cells.

This is the time to mention about my closest friend Praveen Kumar, who has always been there for me whenever I have needed him (though he always comes late but somehow manages to keep the goodwill) and all my lab mates at the Bioengineering Laboratory and Combustion and Laser Diagnostics laboratory for their support.

Finally I would like to acknowledge my parents Mr. K. R. Venkateswarlu and Mrs. M. V. Aruna and my sister K. Mayuri for their support and for making me what I am today.

Table of Contents

List of Tables

List of Figures

Nomenclature

L_p	Plasma Membrane Permeability (μm/min-atm)
A_s	Surface Area (m^2)
R	Gas Constant (8.02e13 μm^3/mol)
T	Absolute Temperature (K)
P_e	Extracellular Vapor Pressure (Pa)
P_i	Intracellular Vapor Pressure (Pa)
V_w	Molar Volume of Water (m^3/mol)
L_f	Molar Latent Heat of Fusion (KJ/mol)
n_2	Osmoles of Solute in The Cell (Osm)
V	Cell Volume (m^3)
B	Cooling Rate (^oC/min)
L_{pg}	Reference Membrane Permeability
E_a	Activation energy of L_p (KCal/mol)
T_R	Reference Temperature (K)
T_{seed}	Seeding Temperature (K)
o	As subscript refers to isotonic conditions
Ω_o	Kinetic Factor
N_s	Number of water molecules in contact with catalytic structure
N_{so}	Number of solute molecules in contact with catalytic structure
η	Viscosity of Cytoplasm (Ns/m^2)
ΔT	T-T_{fusion} (K)
T_m	Melting/Freezing Temperature (K)

α	Thermal Diffusivity (m^2/sec)
$L(r,s)$	Radiance in the radial and transverse directions (W/m^2-Sr)
μ_t	Attenuation Coefficient (1/m)
μ_s	Scattering Coefficient (1/m)
$P(r,s)$	Scattering Phase Function
$d\omega$	Infinitesimal Solid Angle (Sr)
$S(r)$	Rate of Heat Generation (W/m^3)
$\emptyset(r)$	Fluence Rate (W/m^2)
ρ	Density (Kg/m^3)
c	Specific Heat (J/Kg-K)
k	Thermal Conductivity (W/m-K)
s	As subscript indicates solid or frozen section
l	As subscript indicates liquid or unfrozen section
t	Time (sec)
T_m	Phase Change Temperature (K)
T_w	Wall Temperature (K)

Abstract

The importance of the imposed cooling rate in cryopreserving native cells and tissues has been long recognized in the field of cryobiology. When biological tissues are subjected to cooling rates in excess of thousands of degree C per minute, the characteristic structural and physical manifestations of the ice formed are such that the traditional damage due to ice formation at lower cooling rates are suppressed. Hence, achieving high cooling rates in tissues and cells of biologically relevant sizes (mm's and cm's) has been a long standing research problem. In the present study, we present a novel technique to achieve high cooling rates (in the order of 8,000 to 10,000 ^{o}C/min) in large tissue sections by coupling pulsed laser heating and immediate exposure to cryogenic temperatures (liquid nitrogen vapor at -164 ^{o}C). Thermal gradient that exists between the laser heated tissue (at ~1000's ^{o}C) and liquid nitrogen surrounding the tissue results in very high cooling rates, as opposed to the cooling rates experienced by the tissue without laser heating (which is in the order of a few hundreds of degree C per minute). Furthermore it is expected that the small time scales of energy deposition (6-7 ns) and localized heating due to laser focusing would lead to minimal thermal damage. To illustrate this idea we have developed a 1-D and 2-D numerical model to predict cooling rates experienced in a finite tissue section exposed to liquid nitrogen temperatures with and without laser heating. Based on the numerical results preliminary experiments were carried out in a variety of cryobiologically relevant solutions and using adipose tissue derived adult stem cells. Experimental results indicate the possibility of attaining better survival when cells were cryopreserved using the suggested protocol. The limitations and advantages of the technique are also assessed.

Chapter 1

Introduction and Problem Statement

1.1 Cryopreservation

The need for preserving engineered biological tissues and organs is evident from a recent study by Han and Bischof (2004), which clearly elucidates the fact that in 2002, for every organ/tissue donor in United States there were five patients. This situation is often referred to as the "transplantation crisis" and has focused interest on developing new methods which can augment the shortage of native and engineered tissues as well as organs. Cryopreservation is a process where cells or whole tissues are preserved by cooling them to low sub-zero temperatures, such as (typically) -80°C or -196°C (the boiling point of liquid nitrogen). At these low temperatures, any biological activity, including the biochemical reactions that would lead to cell death are effectively stopped (Mazur, 1970). Key issues associated with cryopreservation techniques are to store biological systems in the frozen state for extended peroids of time and, to ensure reproducability of the structural and biophysical parameters on revival. Living cells are highly complex and dynamic structures of tremendous subtlety, but most cells also possess amazing resiliency in the face of challenges to their survival. It is because of this resiliency that the science of cryopreservation is possible.

The phenomena of cryopreservation can be thought of as arising from two contradictory effects of temperature reduction. The most familiar effect of reduced temperatures is a reduction in the rate of deterioration of biological systems. But the other effect is detrimental in nature, and arises not only because of the transformation of liquid water into ice crystals, but also because living systems optimized for survival at

higher temperatures cannot perform self-maintenance functions at lower temperatures. Biological systems encounter phenomena such as phase changes in membrane lipids or cold-induced protein denaturation at lower temperatures for which they have not evolved specific defenses. Cryopreservation as a technique has been applied effectively to preserve a variety of mammalian systems (Mazur, 1984; McGrath, 1985) including erythrocytes or red blood cells, lymphocytes, gametes, micro organisms, isolated tissue cells and small multicellular organisms. Cryopreservation of structurally complex organisms like embryos has also been studied extensively by McGrath (1975) and Mazur (1984). Other important studies include cryopreservation of mammalian sperm (Devireddy *et al*, 2000; Devireddy *et al*, 2002(a); Thirumala *et al*, 2003) and liver slices (Day *et al*, 1999). But the problem of transplantation crisis is yet unanswered due to inadequate protocols to store sizeable tissues and organs. Partly because of the events that occur during freezing of biological systems, which are complicated and are not clearly understood, and also due to lack of techniques to achieve cooling rates which can vitrify biological tissues (Fahy, 1987).

1.2 Problem statement

Freezing biological systems at extremely high cooling rates (1,000's of ^{o}C/min) essentially leads to solidification, attributable to a tremendous elevation in viscosity of the freezing fluid. At such high cooling rates freezing does not occur by crystallization or grain growth, but a second order thermodynamic phase transition leads to an arrest in the translational molecular motions. The frozen region tends to form amorphous ice and is said to have vitrified or formed glass. This work attempts to present an alternative approach to achieve cooling rates of the order of 10,000 ^{o}C/min, by elevating the thermal

gradient of the tissue to be cryopreserved, by irradiating it with an ultra short laser pulse and then exposing it to cryogenic fluid temperatures. Numerical and experimental results indicate the possibility of vitrifying biological tissues using this alternate protocol.

Chapter 2

Background and Review

2.1 Introduction

Water, the major component of cells, when subjected to freezing tends to become ice, which inhibits the cellular metabolism. The nature of ice formed and the rate of formation thus becomes an important parameter in deciding the viability of the cryopreservation protocol (Diller, 1979). The range of temperatures at which the cell (or tissue slices) experience lethal effects is between ~-15 ^{o}C to -60 ^{o}C (Mazur, 1966). Once frozen, cells can endure storage at very low temperatures for a long period of time. This is because no thermally driven reactions occur in aqueous systems at commonly used storage temperatures of -196 ^{o}C and as liquid water does not exist below -130 ^{o}C. At these temperatures the crystalline or glassy states that exist have high viscosities making diffusion effects insignificant over less than geological time spans (Mazur, 1984).

During a freezing process, the extracellular region forms ice first and then the intracellular region begins to change state. This can be attributed to the fact that the cell (typical diameter 50μm) membrane prevents growth of external ice into the region inside the cell (referred to as the intracellular region) making the intracellular region supercooled (~-8 ^{o}C). If the cooling rates are low then the supercooled intracellular region, equilibrates with the surrounding ice by loosing water. This occurs due to the high vapor pressure that develops within the supercooled cell. As a result, the solute concentration within the cell becomes extremely high and the cell dies due to various reasons like dehydration, solute toxicity and cell shrinkage in the presence of hypertonic solutions (Lovelock, 1953). The rate and extent of dehydration depends primarily on two

variables. One is the inherent permeability of cell to water (that is the hydraluic conductivity, L_p) and the other being the cooling rate, B. For a cell of given L_p the slower it is cooled, the more it is able to loose sufficient water in order to remain in near chemical potential equilibrium with external ice and solution. Conversely, if the cooling rates are high but not extremely high (typically ~100 ^{o}C/min-500 ^{o}C/min), the intarcellular water present in the cell nucleates due to its inability to maintain equilibrium with the external environment by exmosis. As a result formation of crystalline ice with sharp edges occurs intracellularly. Furthermore, a sudden volume expansion of the cell leads to a rupture of the cell membrane and eventually, cell death (Ishiguro and Rubinsky, 1994).

This qualitative description of water transport as a function of cooling rates can be quantitatively described by four coupled equations (Mazur, 1963). The first equation relates the rate of loss of cytoplasmic water to the differnece in chemical potentials of the intracellular and extracellular water, expressed as vapour pressure fraction;

$$\frac{dV}{dt} = \left(L_p A_s RT \ln\left(\frac{P_e}{P_i}\right)\right) / v_w \tag{1}$$

The change in the vapour pressure ratio with temperature can be computed from a first order differential equation as derived from the Clausius-Clayperon relation and Raoult's law;

$$\frac{d}{dT}\left(\ln\left(\frac{P_e}{P_i}\right)\right) = \frac{L_f}{RT^2} - \left(\frac{n_2 v_w}{V + n_2 v_w} V\right)\frac{dV}{dT} \tag{2}$$

The time and temperature can then be related to cooling rate which, if linear, is given by;

$$\frac{dT}{dt} = B \tag{3}$$

and finally, the hydraulic conductivity, *Lp*, which decreases with falling temperature is assumed to follow the Arrhenius relation given by;

$$L_p = L_{pg} \exp\left(\frac{-E_a}{R'}\left(\frac{1}{T} - \frac{1}{T_R}\right)\right) \tag{4}$$

The probability of intercellular ice formation in tissues can be modeled using a model originally developed to predict the probability of intercellular ice formation in cell suspensions as shown in Eqn. (5) (Bischof and Rubinsky, 1993; Bischof *et al*, 1997; Devireddy *et al*, 2002; Toner and Cravalho, 1990);

$$PIF = 1 - \exp\left[-\frac{1}{B}\int_{T_{seed}}^{T} A\Omega_o \frac{N_s}{N_{so}}\frac{\eta_o}{\eta}\left(\frac{T}{T_{fo}}\right)^{1/2} \exp\left[-k_o \frac{(T_f / T_{fo})^4}{\Delta T^2 T^3}\right] dT\right] \tag{5}$$

Eqn. (1)-(4) as well as the probability of IIF presented by Eqn. (5) clearly indicates that

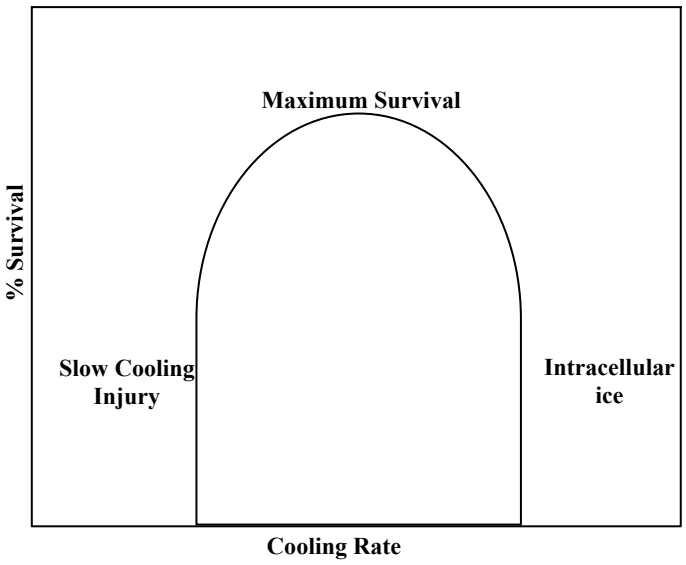

Fig 2.1 Inverse U curve. Effect of cooling rate on the survival of a representative biological cell.

the maximum survival occurs at an intermediate range of cooling rate. Fig 2.1 is the typical repesentative survival curve for any given cell type as a function of its cooling rate. As stated earlier, high and low cooling rates can reduce the post thaw survival of the

cells by intracellular ice formation (IIF) and by solute damage respectively. Based on this, a cooling rate for maximum cell cryosurvival should exist between the high and low rates which is refered to as the optimal cooling rate (cooling rate for maximum survival in Fig 2.1), and has been confirmed experimentally for a variety of cell types. Optimal cooling rates can vary between 1 ^{o}C/min for mouse marrow stem cells (Whittingham *et al*, 1972) to 1,000 ^{o}C/min for human red blood cells (Mazur *et al*, 1970) .

2.2 Changing the paradigm- Vitrification

The simplest way to supress or prevent crystallization of ice in solutions (i.e. vitrify samples at practicable cooling rates) is the use of chemical compunds (cryoprotectants) in very high concentrations. By adding these cryoprotective additives to a cell suspension, the survival following freezing and thawing can be substantially increased. This can be attributed to the changes in the structural and physical characteristics of the ice, that forms in the presence of CPA's. The traditional realm of cryobiology typically works at this optimum cooling rate where the maximum cell survival occurs in the presence of these chemicals called cryoprotective agents (CPA's). Cryoprotective agents can be subcategoarized into penetrating and non penetrating types. Penetrating CPA's are small, nonionic molecules that have a high solubility in water at low temperatures, they lower the concentration of salts normally found in the physiological solutions at a given temperature below the freezing point. Thereby reducing the magnitude of injury and the kinetics at which damage accumalates. Non penetrating CPA's are generally chain like polymers that are soluble in water and have large osmotic co-efficents. They are thought to act by dehydrating the cell before freezing, thereby reducing the amount of water that

the cell needs to lose to remain close to osmotic equilibrium during freezing. The cytoplasm then does not supercool to the same extent, thereby reducing the IIF.

Fig 2.2 shows the supplemented phase diagram for a generic chemical compound in water (Fahy, 1984). As might be expected, different concentrations of the chemical compound result in different regions of behavior in the phase diagram. In Region-1,

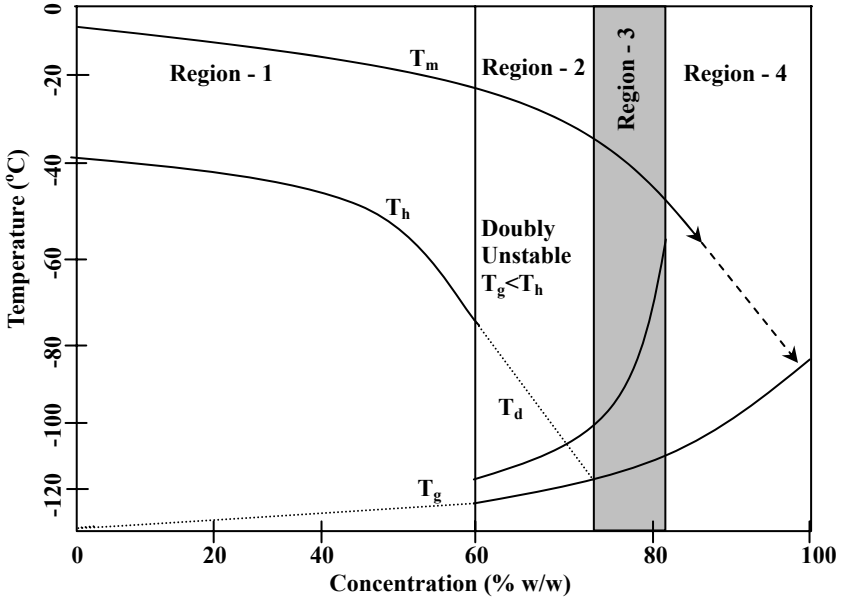

Fig 2.2 Supplemented phase diagram for a typical cryopreservation protocol in the presence of CPA's.

cooling to any temperature below the equilibrium freezing/melting temperature (T_m) results in the formation of ice crystals due to the presence of impurities or heterogeneous nucleating agents. In the absence of impurities, homogeneous nucleation of ice occurs at a well defined temperature (T_h). Thus there is no clear way to suppress the formation of ice crystals in Region-1 (with the exception of imposing very high cooling rates that are currently impracticable in large samples). Region-1 is comparable to traditional cryopreservation process in that the concentration of chemicals used is low and non-toxic. At higher concentrations (Region-2), cooling rates achievable by quenching of

small samples allow the apparent vitrification of the sample (Boutron, 1986; MacFarlane, 1987). In this region, the sample remains transparent to eye rather than white and opaque after cooling to a temperature below the glass transition temperature (T_g). Nevertheless, it is likely that ice crystal nuclei will form in such solutions, even if the nuclei are unable to grow to visible size (Fahy, 1988). Thus Region-2 is called "doubly unstable" because the ice formed is not only thermodynamically unstable but is also unstable by virtue of $T_g<T_h$ (Fahy, 1988). At the high concentration limit of Region-2, $T_g \sim T_h$, the heterogeneous nucleation can be transcended in much more the same way as homogeneous nucleation is transcended in Region 2. Thus, in Region-3, the formation of a vitreous state intervenes to make ice crystallization impossible (i.e. both the homogeneous and heterogeneous nucleation of ice is suppressed). The concentrations which is equal to the boundary between Region-2 and Region-3 is referred to as C_v, i.e. the lowest concentration supporting the apparently complete vitrification. At C_v, T_g is achieved without encountering T_h and in general ranges from 40%-60% weight to volume ratio (Fahy, 1988). Concentrations in Reigion-4 would be very stable in terms of ice formation and are ideal for vitrification of samples. Paradoxically, although the concentrations of CPA's in Region-4 tend to enhance the survival of cells in lieu of the thermodynamically stable ice that forms in this region (which and is devoid of any nucleation) thus ideal for vitrification but then again the overwhelming chemical toxicity to which lving systems are subjected to, limits its practical application for cryopreservation.

An ideal combination of traditional cryopreservation processes (Region-1) and vitrification processes (Region-4) will either diminish the overwhelming chemical

toxicity to living systems in Region-4 (as pursued by a variety of investigators, including Fahy and his coinvestigators for the last 20 years; Fahy *et al* 1984; Fahy 1998) or supress the fomration of ice crystals by imposing very high cooling rates in Region-1 (as proposed in the current study).

2.3 Cryopreservation at ultra-high cooling rates

Freezing biological systems at extremely high cooling rates (1,000's of ^{o}C/min) essentially leads to solidification, attributable to a tremendous elevation in viscosity of the freezing fluid. At such high cooling rates freezing does not occur by crystallization or grain growth, but a second order thermodynamic phase transition leads to an arrest in the translational molecular motions. The frozen region tends to form amorphous ice and is said to have vitrified or formed glass. Vitrification is a technique whereby biological systems can be stored as amorphous (ice free) solids at temperatures below the glass transition either by manipulating both the cooling rate and the concentration of CPA's (usually 6~8 M) or occasionally by modifying the pressure. Vitrification was originally proposed by Luyet (1937) and can remove the risk of ice crystal formation within the biological systems during cryogenic preservation. This process fundamentally differs from most cryopreservation techniques where crystallization and grain growth are considered as natural byproducts of the freezing protocol. Any damage due to IIF and high concentration of extracellular solutions (solution effects), that occur during a typical cryopreservation protocol are also avoided. However using traditional cryopreservation techniques has led to difficulties related to effective loading and unloading of high concentrations of CPA's as well as the apparent need of high pressures to make this protocol possible in whole tissues. Any protocol where entire tissue/organ can be frozen

at cooling rates of the order of ~10,000 ^{o}C/min would be an ideal cryopreservation protocol and could potentially address transplantation crisis issues effectively.

Cooling rates experienced by biological systems are a function of its thermophysical properties (thermal diffusivity (α) and the latent heat of fusion (*L*)) as well as the imposed thermal gradient. Traditional cryopreservation techniques as explained in the earlier section alter the thermophysical properties, either by increasing the thermal diffusivity or by decreasing the amount of latent heat released to achieve

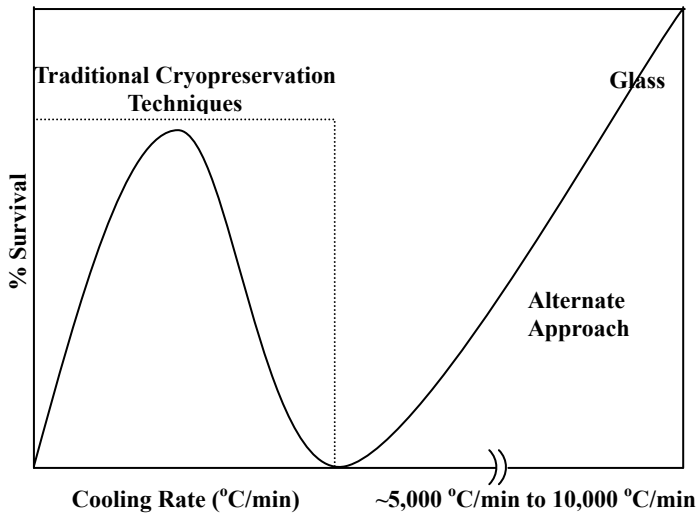

Fig 2.3 Representative cell survival at extremely high cooling rates (~5,000 ^{o}C/min to 10,000 ^{o}C/min)

higher cooling rates. An alternate approach qualitatively presented in Fig 2.3 could be to alter the thermal gradient of the system instead of changing the biophysical attributes of the cell. The work reported on injecting water drops at high pressure into the cryogenic fluid (Mayer, 1985), subjecting of crystal ice to very high pressures until it collapses (Johari *et al*, 1990; Handa and Klug, 1988), and water being vapor deposited at low pressures into cold plates (Hallbrucker *et al*,1989) have all tried in some way or the other to alter the thermal gradient imposed on the freezing systems with limited success. These

experiments have shown that amorphous solid water can be created directly from liquid water when cooling rates greater than 10,000 ^{o}C/min are applied to the system.

As the temperature of the cryogenic fluid (liquid nitrogen) cooling a biological system is limited to -164 ^{o}C in the vapor form or -196 ^{o}C at its boiling point, the only other means to alter the thermal gradient could be by elevating the temperature of the system itself. Altering the thermal gradients by elevating the temperature of biologically relevant solutions, and then bringing them in contact with cryogenic fluid (liquid nitrogen at -164 ^{o}C) was originally proposed by Fowler and Toner (1997). They conducted experiments in layers of aqueous sucrose solution sandwiched between two parallel glass plates and could achieve some transparent regions in the frozen solution. The results were not conclusive as some transparent regions could be obtained during traditional cryopreservation protocols, even at low cooling rates. The mathematical description of the physical phenomena was not presented clearly and any phase change effects in the freezing solution was neglected. Following the idea conceived by Fowler and Toner (1997), this work attempts to present an alternative approach to achieve this glass transition in freezing biological systems. The temperature of the tissue to be cryopreserved is elevated by an ultra short laser pulse and then the heated tissue brought in contact with liquid nitrogen. Subsequent section presents a discussion on using commercially available lasers as heat sources.

2.4 Lasers as heat sources

Pulsed laser heating of biological systems has shown that upon sudden removal of laser heating, thermal conduction with the surrounding region, results in extremely high cooling rates (Fowler and Toner, 1997). The advantage that laser heating has over other

techniques is that tremendous amount of energy can be deposited into the system within very short periods (6~7 nsec) and has been used for targeted tissue ablations, also a radiation trap can be created where the energy can be uniformly deposited within the system which is to be heated. The development of a unified theory for the optical and thermal response of tissue to laser radiation is still in its infancy. Tissue is an absorbing and scattering medium in which the incident light propagates. Since the optical and thermal responses of tissue to laser irradiation are highly dependent upon the characteristics of the laser source it is imperative to describe various laser parameters and their influence upon the tissue response. Basic irradiation parameters affecting the heat transfer in tissue using pulsed lasers as heating sources are the energy per pulse, irradiation time, spot size, repetition rate, and number of pulses. The spectrum of commercially available lasers for diagnostic and therapeutic medical applications stretches from 193nm to 10.6 μm. Since absorption and scattering of any tissue varies with the incident wavelength, there are dramatic differences in the penetration depth of the irradiance from various lasers (Walsh, 1995). Light at either 193 nm or 296 nm is totally absorbed in the first μm of the tissue owing to the amino acid absorption in the UV and water absorption in the IR. In contrast, light from 500nm to 110 nm can penetrate several millimeters in tissue and can lead to temperatures of the order of 1,000 ^{o}C locally. As the collimated beam passes through tissue, it is exponentially attenuated by absorption and scattering (Gardner *et al*, 1996). The scattered light forms a diffuse volume around the collimated beam and heat is generated wherever collimated or diffuse light is absorbed. Increasing the tissue temperature also increases the reaction rates that can lead to tissue denaturation. Thus the computation of damage requires accurate

predictions of temperature with time, which again requires knowledge of the rate of heat production. Heat generation in turn is dependent upon an accurate estimate of the fluence rate throughout the tissue. All these computations require specification of laser parameters at the site of radiation and knowledge of the optical and thermal properties and rate constants of the tissue. The transport phenomena associated with the interaction of laser beam and bio material can be divided into three parts:

1. Absorption of some of the laser beam energy;

$$\frac{dL(r,s)}{ds} = \mu_t L(r,s) + \mu_s \int_{4\pi} P(r,s)L(r,s)d\omega \tag{6}$$

2. Conversion of this energy into chemical energy and/or into heat, and diffusion of heat away from the irradiated zone;

$$S(r) = \mu_a(r)\phi(r) \tag{7}$$

$$\rho c \frac{\partial T(r,t)}{\partial t} = \frac{\partial}{\partial r}\left(k \frac{\partial T(r,t)}{\partial r} \right) + S(r) \tag{8}$$

$$E(x,y,z) = E_o(x,y)e^{-\mu_t z} \tag{9}$$

3. Eventually, chemical reaction and/or phase transformation (in general, vaporization);

$$\Omega(r,t) = A\int_0^t \exp\left(-\frac{\Delta E}{RT(r,t)} \right) dt \tag{10}$$

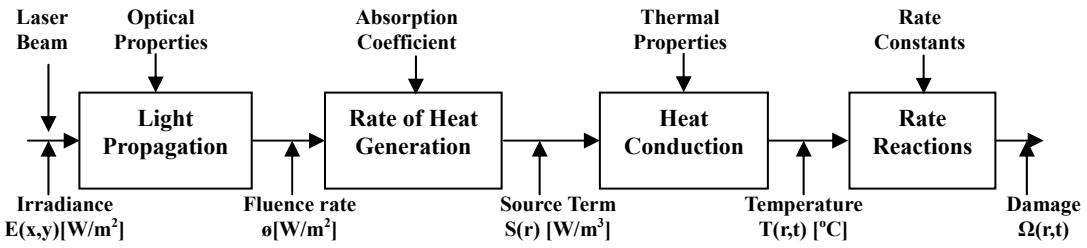

Fig 2.4 Transport phenomena during a typical laser material interaction. For the case of a laser heated tissue dipped in liquid nitrogen, high cooling rates can be achieved.

Once the laser flux is deposited into the tissue, thermal diffusion follows the standard Fourier heat conduction model if the thermal relaxation time within the biomaterial is zero else a Non-Fourier heat conduction model describes the thermal diffusion phenomena (Deng and Liu, 2003). Fig 2.4 generically describes the thermal transport phenomena occurring during the interaction of radiation with any material. Depending on the diffusion characteristics, the laser irradiated tissue at an elevated temperature when brought in contact with the cryogenic fluid, experiences huge thermal gradient leading to a quenching like phenomena by virtue of the high cooling rates. The subsequent section presents various mathematical models for predicting the transport of heat in tissues by taking into account the phase change phenomena that occurs during solidification/freezing of the water in the tissue.

2.4 Mathematical models for heat transfer in biomaterials

In cryopreservation, the goal is to achieve controlled and uniform thermal history within the tissue. This is motivated again by the biophysics already discussed, which suggest that extremely high cooling rates (~10,000 ^{o}C/min) will reduce the solution effect injury and IIF. The problem with this approach is that bulk systems will freeze from outside in. In this case the cooling rates will gradually decrease as the interface moves from the edge of the tissue towards the symmetric center. Heat transfer work in cryopreservation has thus centered on estimation of cooling rates within the cylindrical and cartesian co-ordinate system frame work (Hayes *et al*, 1986; Hayes *et al*, 1988; Hartmann *et al*, 1991). Non dimensional treatment of the freezing process (Rubinsky and Cravalho, 1984) and an approach based on time or temperature averaging of cooling rates has also been extensively studied (Hayes *et al*, 1984). Recently Devireddy *et al* 2002 (c)

have reported the effect of microscale heat and mass transfer phenomena on the macroscale response. Notable analytical solutions of heat transfer during phase change exist for well known Stefan and Neumann problems which involve, initially an unfrozen phase which changes to a frozen and unfrozen phase, with a moving interface in between them. The Stefan problem solves for the temperature in the frozen phase only, while the temperature of the liquid is assumed to be at the melting temperature of the substance. The Neumann problem allows for temperature distributions in both the solid and liquid phase. In this case the heat energy, passing through the interface, from solid to liquid is balanced by the evolution of latent heat. Both of these problems are classical conduction problems and are called moving boundary problems (Alexiades and Solomon, 1993; Carlslaw and Jaeger, 1959; Lunardini, 1981; Ozisik, 1993). Although analytical approaches are very useful for broadly understanding the system behavior, they fall short of accurate prediction in biomedical systems. At temperatures greater than -150 ^{o}C water in the tissue can change thermal properties significantly, secondly the temperature dependence of latent heat differs significantly from pure substances, thirdly the geometries involved may be irregular or could be comprised of several different systems with different thermal properties. Again density changes between the solid and liquid states do occur, which has been incorporated in very few analytical models (Alexiades and Solomon, 1993). This calls for numerical approaches to fully understand cryogenic behavior in biological systems.

The numerical approaches used to study heat transfer problems in cryobiology are the front tracking techniques, enthalpy techniques (explicit or apparent heat capacity), and the discrete source term approach. Table 2.1 presents the governing equations applicable

to each technique. In front tracking models (Rubinsky and Cravalho, 1981) one can use the conduction model for the solid and liquid phase with appropriate phase thermophysical properties. For the interface itself, an energy balance between the solid and liquid state is necessary. This can be thought of in terms of the amount of energy removed from the interface being balanced by the amount of heat liberated at the interface. The enthalpy method can be used for either pure or impure solutions in cryopreservation (Hayes *et al*, 1988; Hartmann *et al*, 1991) for accurate representation in terms of the enthalpy function for the material changing phase in both the solid and liquid state. The discretized energy balance is solved to find the enthalpy distribution throughout the medium and the temperature distribution can be calculated from the enthalpy. The enthalpy formulation can also be adapted for use with media in which phase change occurs over a range of temperatures usually ranging from -0.53 ^{o}C to -21.5 ^{o}C (eutectic temperature of water and NaCl). A small modification of this technique is the apparent heat capacity method where the temperature dependence of latent heat can be used to compute the cooling rates (Hayes *et al*, 1986). Lastly in the discrete source approach the left hand side of the formulation represents the change in internal energy in a small region of the medium during a small period of time dt . The net amount of heat added or removed by the neighbouring small regions of medium plus the heat released inside the small region of medium due to phase change during time dt is given on the right hand side of the equation. The source term exists only if the phase change occurs otherwise it is zero. One or more techniques mentioned above could be used to solve the transport equations in subsequent chapters. The laser flux would be used as source terms

in the transport equations and appropriate cooling rates would be evaluated in dimensionally large tissues sections. It is expected that the cooling rates achieved by this

Table 2.1 Numerical approaches used in solving phase change problem

Method and equation	*Latent heat condition*
1. Front tracking method (*i* solid or liquid) $\rho_i c_i \frac{\partial T_i}{\partial t} = \frac{\partial}{\partial x_j}\left(k_i \frac{\partial T_i}{\partial x_j}\right)$	$k_s \frac{\partial T_s}{\partial \bar{x}} - k_l \frac{\partial T_l}{\partial \bar{x}} = \rho_s L \frac{\partial \bar{x}}{\partial t}$
2.1 Enthalpy method $\frac{\partial(\rho h)}{\partial t} = \frac{\partial}{\partial x_j}\left(k \frac{\partial T}{\partial x_j}\right)$	$h = \begin{cases} c(T - T_s)\ where T \le T_s \\ \Lambda L\ where\ 0 \le \Lambda \le 1, T_s < T \le T_l \\ c(T - T_l) + L\ where\ T > T_l \end{cases}$
2.2 Apparent heat capacity method $\rho\left[c + L\frac{\partial \Lambda}{\partial T}\right]\frac{\partial T}{\partial t} = \frac{\partial}{\partial x_j}\left(k_i \frac{\partial T}{\partial x_j}\right)$	$\frac{\partial \Lambda}{\partial t} = \frac{\partial \Lambda}{\partial T}\frac{\partial T}{\partial t}$
3. Discrete source term $\frac{\partial(\rho c T)}{\partial t} = \frac{\partial}{\partial x_j}\left(k_i \frac{\partial T}{\partial x_j}\right) + S$	$S = f(L, \Lambda, T, t)$

protocol would help in suggesting an alternative approach to vitrify biological tissues and address the problem of transplantation crisis effectively.

2.5 Objectives of the present work

1. To develop a one dimensional computational model of tissue section irradiated by an ultra-short laser pulse and exposed to cryogenic fluid and to evaluate the cooling rates in the tissue section. Temperature dependent thermophysical properties of the frozen section are taken into account while developing the model and the phase change is assumed to occur at -0.53 ^{o}C.

2. To extend the model to a two dimensional framework and accurately predict cooling rates in laser irradiated tissue sections exposed to cryogenic fluid, by taking into account temperature dependence of latent heat (true for all isotonic solutions).
3. To conduct a brief analysis of the current protocols viability in terms of thermal damage caused due to the laser irradiation.
4. To conduct preliminary experiments on various cryobiologically relevant solutions and to qualitatively determine the formation of glass when the solutions are subjected to high cooling rates using the suggested protocol. Percentage survival test on actual living cells would also be conducted for the case of adipose tissue derived adult stem cells.

Chapter 3

Numerical Investigation of a Novel Method to Vitrify Biological Tissues Using Pulsed Lasers and Cryogenic Temperatures*

3.1 Motivation

Vitrification has shown great promise to improve freeze-storage protocols for biological systems (Fahy and Hirsh, 1982; Fahy *et al*, 1984; Fahy 1998). Vitrification is essentially solidification of liquid, by an extreme elevation in viscosity and not by ice crystallization (Fahy, 1998; Doremus, 1973; Kauzmann, 1948). During the process of vitrification the solidified solution tends to become glass wherein the translational molecular motions are significantly arrested marking an effective end of biological time, without the deleterious changes associated with ice crystal formation. This differs from traditional cryopreservation process, where crystallization and growth of ice in the freezing medium, is considered as a natural byproduct of the storage technique. Vitrification as a process eliminates the formation of damaging intracellular ice as well as long-term exposure to highly concentrated extracellular solutions (Fahy *et al*, 1984; Fahy, 1998; Doremus, 1973; Kauzmann, 1948; Mazur, 1994; Mazur 1970). Further use of vitrification as a storage technique is hampered by a lack of techniques to achieve high and uniform cooling rates of the order of ~10,000 ^{o}C/min in large tissue sections (Fahy *et al*, 1984; Fahy, 1998; Mazur, 1994; Mazur, 1970).

3.2 Introduction

The cooling rates experienced by a tissue during a freeze protocol are a function of the thermophysical properties (α and L) of the tissue being frozen, and the imposed temperature gradient. Decreasing the value of L, and increasing the value of α along with

the imposed thermal gradient will increase the cooling rates experienced by the tissue. Since the thermo-physical properties of the tissue are difficult, if not impossible, to modify, we propose to increase the thermal gradient. The thermal gradient is defined as the temperature difference between the cryogenic fluid (typically liquid nitrogen temperature or –196 ^{o}C) and the body temperature. Clearly, the only way to increase the thermal gradient (and the cooling rate experienced by the tissue) is by increasing the body temperature, through the use of lasers (Jacques and Prahl, 1987; Pearce and Thomsen, 1995).

We propose in the current study to investigate the use of commercially available lasers as a means to deposit thermal energy in extremely small durations, uniformly throughout the tissue section to be vitrified. It is hoped that the small time scales of energy deposition will mitigate the laser induced thermal damage in the tissue cells (Jacques and Prahl, 1987; Pearce and Thomsen, 1995). Since, the idea is relatively new (originally expounded by Fowler and Toner, 1997), we propose to develop a simple one-dimensional model to qualitatively understand thermal history, freezing rates and cooling rates within a tissue section of finite dimension, irradiated by a laser pulse and immediately exposed to cryogenic temperatures. To this end, we present in the following sections a mathematical model, a description of our model parameters along with our numerical techniques and results.

3.3 Mathematical model

Devireddy *et al* (2002 (c)) have previously presented a tissue freezing model that accounts for the effect of microscopic heat transfer phenomena on the macroscale tissue freezing response (thermal history, freeze front, etc.). Based on these earlier results by

Devireddy *et al* (2002 (c)) that suggest that the macroscale results are not affected by the microscale phenomena, we propose in the present study to simulate tissue freezing using the standard one-dimensional Fourier heat conduction equation described as,

$$\frac{\partial(\rho c T)}{\partial t} = \frac{1}{r^n}\frac{\partial}{\partial r}\left(r^n k \frac{\partial T}{\partial r}\right); \tag{1}$$

where the parameter *n* defines the coordinate system, i.e. *n* being equal to either 0 or 1 or 2 transforms Eqn. (1) into cartesian, cylindrical or spherical coordinate system respectively. The tissue parameter (α) is assumed to be a function of temperature as shown in Table 3.1 (Devireddy *et al*, 2002 (c)). However, for simplicity we assume that α is constant and independent of temperature in the unfrozen tissue (Table 3.1). And finally, for a simplified analysis of the freezing process we assume that the phase transition takes place at a fixed temperature of –0.53 ^{o}C.

Assuming that the thermal wave propagates at infinite velocity within the tissue section, Eqn. (1) for the frozen region is (Devireddy *et al*, 2002 (c); Rubinsky and Cravalho, 1981; Hayes and Diller, 1983),

$$\frac{\partial T_s}{\partial t} = \alpha_s \frac{\partial^2 T_s}{\partial x^2}; t > 0, 0 < x < s(t); \tag{2}$$

where the position of phase change interface *s(t)* is given by,

$$s(t) = \int_0^t V dt; \tag{3}$$

similarly, the governing equation for the unfrozen tissue section is given by Eqn. (4),

$$\frac{\partial T_l}{\partial t} = \alpha_l \frac{\partial^2 T_l}{\partial x^2}; t > 0, s(t) < x < d; \tag{4}$$

The initial and boundary conditions for the tissue section are,

$$T = T_o \; ; t = 0 \, , 0 < x < d \; ; \tag{5}$$

$$T = T_w \; ; t > 0 \, , x = 0 \; ; \tag{6}$$

$$\frac{\partial T_l}{\partial x} = 0 \; ; t > 0 \, , x = d \; ; \tag{7}$$

A single temperature representing the phase change temperature replaces the temperature discontinuity at moving phase interface as,

$$T_s = T_l = T_m \; ; t > 0 \, , x = s(t) \; ; \tag{8}$$

And finally, the continuity of energy balance at the interface requires that

$$k_s \frac{\partial T_s}{\partial x} - k_l \frac{\partial T_l}{\partial x} = \rho L V \; ; t > 0 \; ; \tag{9}$$

Clearly, tracking the phase front, *s(t)* as a function of time will enable us to determine the thermal history within the freezing tissue.

3.4 Laser heating & cryogenic temperatures

As stated in the introduction, the purpose of our study was to investigate the effect of laser heating coupled with cryogenic temperatures to increase the thermal gradient (and consequently the cooling rates) experienced by tissues. To account for the presence of laser heating, the governing equations had to be altered. The intensity of a laser is given as (Jacques and Prahl, 1987; Pearce and Thomsen, 1995; Cammarata and Wautelet, 1999),

$$I_o = \frac{P}{A} W/m^2 \; ; A = \frac{\pi d_b{}^2}{4} m^2 \; ; \tag{10}$$

Where the peak power, P is given by the following equation,

$$P=\frac{E}{t_p}W; \tag{11}$$

In light-tissue interactions only the absorbed light is used to generate heat within the tissue. Typically this energy is either absorbed by the water in the tissue or by hemoglobin in the blood or by melanin in the skin (Cammarata and Wautelet, 1999). If a light beam of intensity I_o hits the medium of thickness x then the intensity I at the output of the medium is given by

$$I(x) = I_o(1-R)\exp(-\alpha_c x); \tag{12}$$

for water typical values of R are ~0.019 and α_c are ~50 μm (Cammarata and Wautelet, 1999). The laser energy input in our study is assumed to be an argon ion laser working at a peak power of 5MW with pulse duration of 2.0 nsec at a wavelength of 488 nm and an exit beam diameter of 2 mm. Pulsing only increases the net instantaneous energy deposited and bears no effect to the temporal resolution of grid.

The governing equation (Eqn. 2) for the frozen region is now modified to account for the presence of laser energy input as,

$$\frac{\partial T_s}{\partial t} = \alpha_s \frac{\partial^2 T_s}{\partial x^2} + I(x); \tag{13}$$

Similarly the governing equation for the unfrozen part is,

$$\frac{\partial T_l}{\partial t} = \alpha_l \frac{\partial^2 T_l}{\partial x^2} + I(x); \tag{14}$$

Note that the initial and the boundary conditions are not affected by the presence of the laser heating (treated in our model as an instantaneous energy/source term at time $t = 0$). Clearly, once the energy gets deposited within the tissue surface, the governing equations

revert to those presented earlier, albeit with the initial temperature of the tissue being a non-uniform value throughout the tissue due to the energy deposited by the laser.

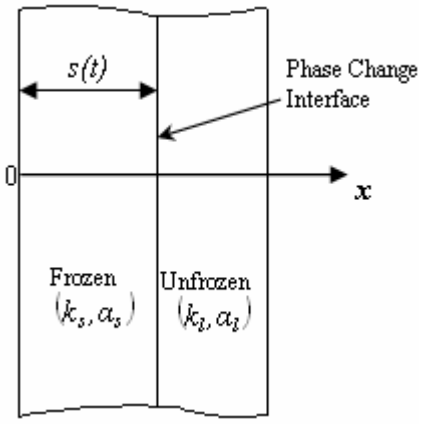

Fig 3.1 Represents the geometry of the freezing tissue section.

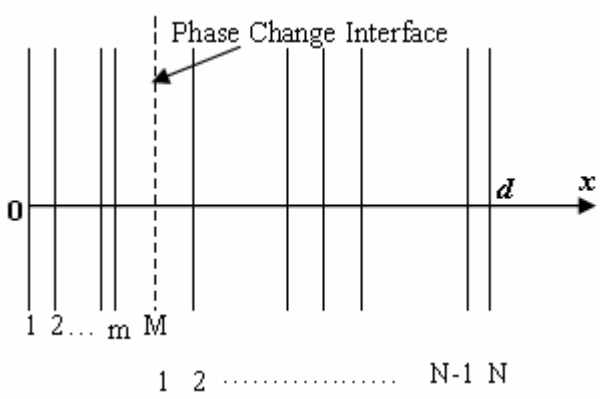

Fig 3.2 The subdivision of the *x* domain

3.5 Numerical solution

In the present study moving grids are utilized along with a control volume based approach (Patankar, 1980; Jo *et al*, 1999). The spatial and temporal discretizations are based on instantaneous phase velocity (see Figs 3.1 and 3.2 for a pictorial description of the computational domain). A second order accurate, implicitly stable Crank-Nicholson method was used in time to predict the thermal history. The Crank-Nicholson method being used, is an unconditionally stable scheme for all discretizations, spatially as well as temporally and is an ideal method for moving grids. The temperature dependent thermophysical properties for the frozen region are evaluated using the model predicted temperature at the previous time step. This assumption was validated by comparing the model simulations at various time step increment values, *dt*. Since, a large *dt* reduces the computational time and a small *dt* increases the accuracy of the model results, an optimal value (or the highest value) of *dt* (= 0.1 secs) that did not significantly (~±0.05%) alter the model results was chosen.

Table 3.1 Thermophysical and other constants in Eqns. (2)-(9)

Thermophysical Constant	Value and units
k	0.6 W/m-K (unfrozen) $2.24+0.005975(273-T)^{1.156}$ W/m-K (Frozen)
C_p	4200 J/Kg-K (unfrozen) 7.16T+138 J/Kg-K (frozen)
ρ	999 Kg/m^3 (unfrozen) 921 Kg/m^3 (frozen)
L	335 J/kg
T_m	-0.53+273 K
T_w	-163+273 K
T_o	37+273 K

The moving grid formulation utilized in the present study is shown in Fig 3.2. In our model the grid spacing keeps varying at each time step. For computational simplicity the frozen and the unfrozen domains were each separated into 50 grids. The node separating the frozen and unfrozen domain represents the phase front. Tracking this phase front node as a function of time determines the instantaneous locations of the frozen and the unfrozen domains within the tissue. However, the unknown trajectory of the moving interfacial boundary makes the phase change problem a non-linear one and was solved using an iterative algorithm (Jo *et al*, 1999), as described below:

1. Assume an initial velocity of the moving boundary V_o at the beginning of the first time step Γ^1.

2. Calculate the moving interface at time Γ^i (i = 1,2,3) based on V_o.

3. Then solve for the temperature fields in the frozen and unfrozen regions and calculate the new velocity V_o^i at the present location.

4. Determine the corrected velocity, $V = V_o + \gamma(V_o^i - V_o)$ where $0 < \gamma < 1$ is the relaxation factor.

5. Check for convergence: if $\frac{|V_c - V_o|}{|V_c|} > \varepsilon_{\max}$ (where ε_{max} is a prescribed maximum acceptable error 10^{-6} for our study), set $V_o = V_c$ and continue the iterative operation from step 2 until the relative error becomes less than or equal to ε_{max}.

6. If convergence is achieved record the position and velocity of phase change front at the actual time step and then update the temperature fields. Continue to the next time step with $V_o = V_c$.

3.6 Numerical results

Our model was benchmarked against the classical solution of Stefan (Carslaw and Jaeger, 1959), as well as that of Hayes and Diller (1998) and Rubinsky and Cravalho (1981) (Fig 3.3). Under similar initial and boundary conditions, the numerical results

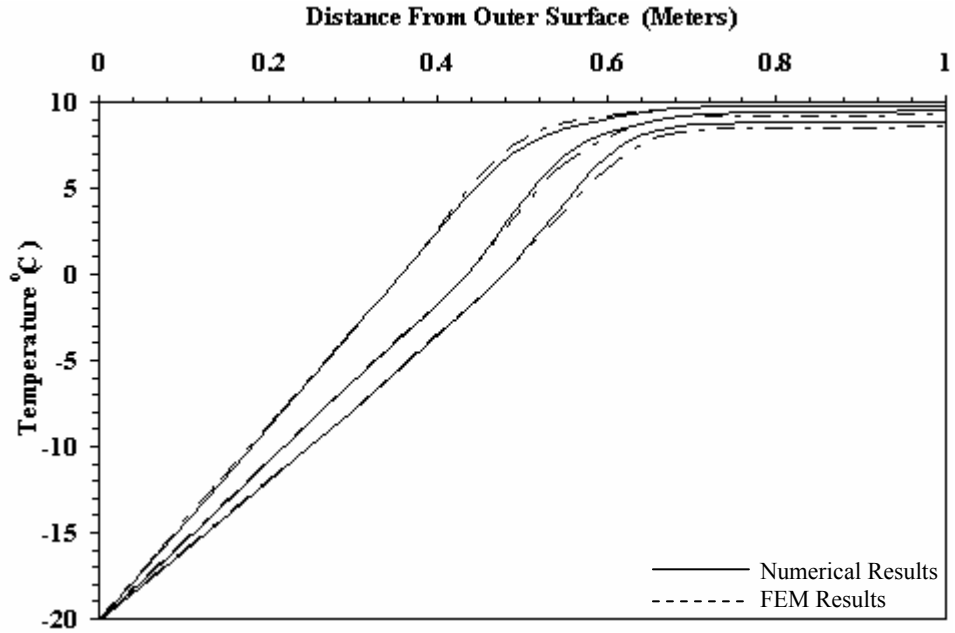

Fig 3.3 Comparison of the predicted temperature distribution in a freezing domain with the finite element results by Rubinsky and Cravalho 1981. The numerical results are in close agreement to the FEM results (98%).

from the present study deviated by <2% from that obtained by the previously published studies (Rubinsky and Cravalho, 1981). The non dimensional temperature distribution is presented in Fig 3.4 where the non dimensional parameters were chosen as;

$$\theta = \frac{T - T_m}{T_o - T_m},\ \Gamma = \frac{\alpha_s t}{d^2},\ X = \frac{x}{d} \tag{15}$$

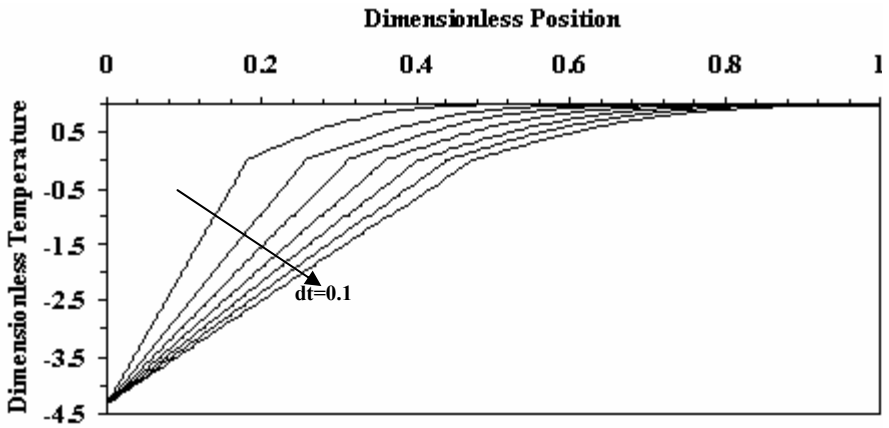

Fig 3.4 Non dimensional temperature distribution with the freezing tissue, note that the discontinuity represents the phase front.

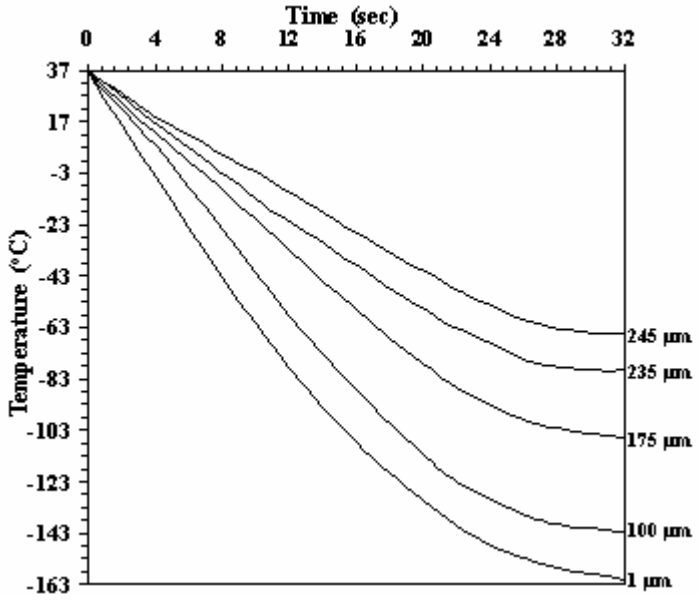

Fig 3.5 Thermal history at five different locations within the tissue section initially at 37 ^{o}C exposed to an ambient atmosphere at -163 ^{o}C. The innermost and outermost locations specify the maximum and minimum cooling rates that the tissue experiences.

The thermal history and cooling rates as predicted by our numerical model, where a tissue (0.5 cm) initially at 37 ^{o}C is brought into contact with liquid nitrogen (-163 ˚C) are shown in Figs 3.5 and 3.6. For a location very close to the surface of the tissue (at 1μm) the cooling rate is ~38 ^{o}C/min and ~18 ^{o}C/min at the line of symmetry (or ~2.45μm into

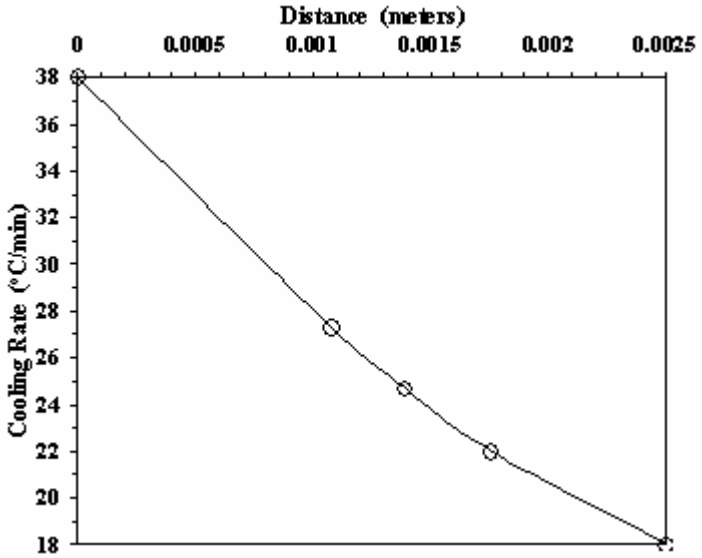

Fig 3.6 Cooling rates at five different locations in a 2.5mm thick tissue initially at 37 ^{o}C when exposed to ambient atmosphere of -163 ^{o}C

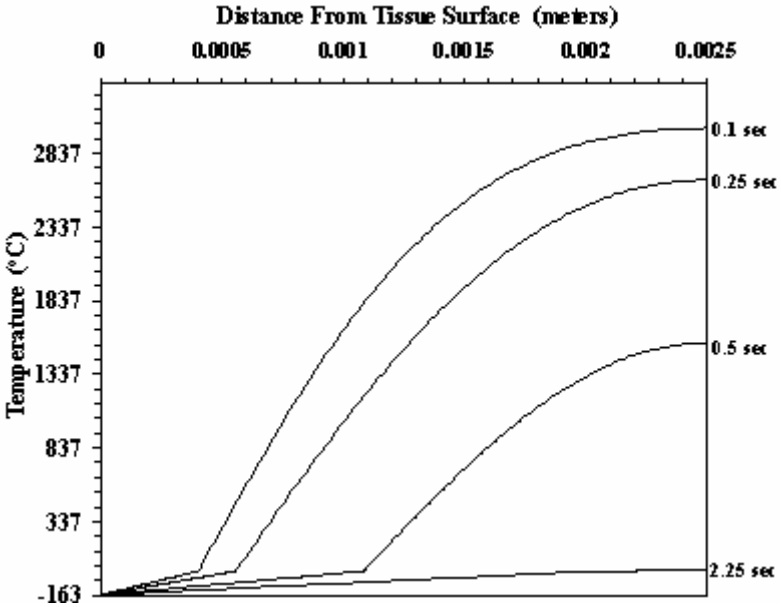

Fig 3.7 Temperature distributions within the tissue section exposed to laser irradiance of wavelength 488nm beam diameter 2mm, pulse duration of 2 nsec and power of 5MW.

the tissue), for temperatures ranging between -0.53 ^{o}C and ~-100 ^{o}C. Clearly, these cooling rates are not significantly "high enough" to vitrify the tissue section, even at the point closest to the liquid nitrogen temperature. The five data points shown in Fig 3.6 are the locations where the cooling rates have been numerically evaluated. Fig 3.7 depicts the temperature distribution within the tissue section after the laser energy is deposited in the tissue. The entire irradiated tissue section has a non-uniform initial temperature distribution as opposed to the earlier case when it was assumed to be at a uniform temperature of 37 ^{o}C. For the laser energy deposition conditions described earlier, maximum temperature that tissue experienced was ~3100 ^{o}C (as shown in Fig 3.7). When the laser irradiated tissue section is brought into contact with liquid nitrogen the high thermal gradient results in cooling rates of the order of ~11,000 ^{o}C/min for a

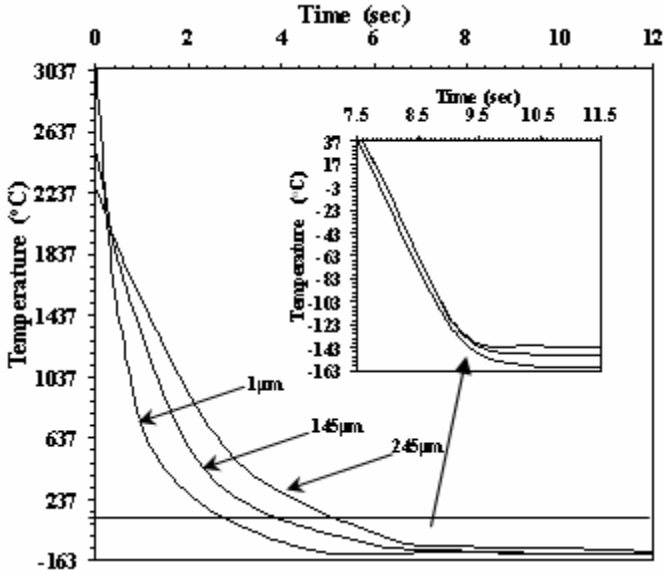

Fig 3.8 Thermal history at three different locations within the tissue section after it is exposed to laser irradiance of wavelength 488nm, beam diameter 2mm and pulse duration of 2 ns under cryogenic temperatures

location very close to the surface of the tissue (at 1µm) and ~9500 ^{o}C/min at the line of symmetry for temperatures ranging between -0.53 ^{o}C and -100 ^{o}C (the resulting thermal

history throughout the tissue and cooling rates as shown in Figs 3.8 and 3.9, respectively; note that for a easy comparison the cooling rates in the irradiated tissue are shown at the same five locations as Fig 3.6). Clearly, the cooling rates shown in Fig 3.9 (~10,000 ˚C/min) are significantly "high enough" to vitrify a large (0.5 cm) tissue section. However, as shown in Fig 3.8, a significant portion of the tissue section experiences very high residence time (~6 secs) at very high temperatures (>100 ˚C). This will clearly damage the tissue via hyperthermic injury and tissue ablation (Cammarata and Wautelet, 1999; Walsh, 1995). This high temperature thermal damage needs to be mitigated before the procedure described in the present study can be considered a viable candidate for vitrifying tissue sections and would be a topic of discussion in further Chapters.

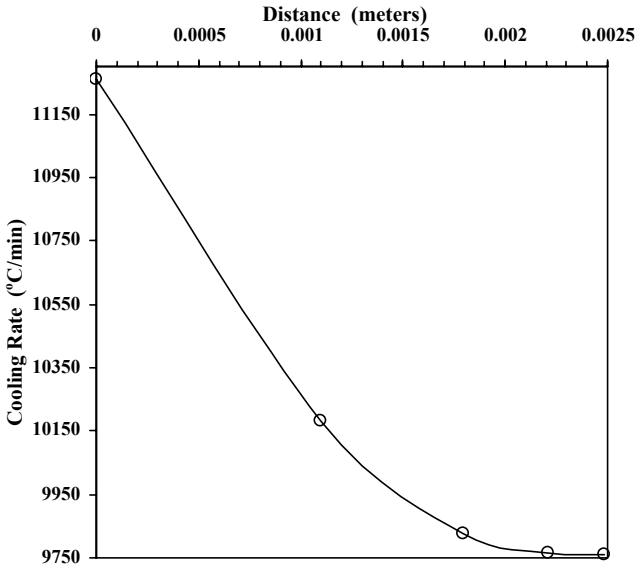

Fig 3.9 Cooling rates at four different locations in a 2.5mm tissue initially at a non uniform temperature when exposed to laser irradiation

3.7 Discussion

A one dimensional numerical model was developed to simulate and predict the thermal history and the cooling rates in a tissue section irradiated by laser and exposed

immediately to cryogenic temperatures. The model results support the possibility of using pulsed lasers and cryogenic temperatures to vitrify large tissue sections. However, further studies are clearly needed to validate the numerical results and refine the model.

Chapter 4

Tissue Interactions with Lasers and Liquid Nitrogen: An Approach to Achieve Very High Cooling Rates (Temperature Dependence of Latent Heat)

4.1 Introduction

Cooling rates experienced by biological systems are a function of its thermophysical properties, the thermal diffusivity (α) and the latent heat (*L*) as well as the imposed thermal gradient on the system. In Chapter 3 a one dimensional computational model of a freezing tissue section with temperature dependent thermophysical properties was developed. It was seen that for millimeter sized tissue sections, it is possible to achieve cooling rates of the order of 10,000 ^{o}C/min by laser heating the tissue and exposing it to cryogenic temperatures. One of the significant assumptions made while developing the computational model was that, latent heat released was independent of temperature and was released at a single phase change temperature of -0.53 ^{o}C. This assumption is valid for pure solutions but for biological tissues which are composed of cells, which contain isotonic solutions, the latent heat is released over a wide range of temperatures. The effect of this phenomenon can be seen quantitatively by Eqn. (1)-(3).

As explained in Chapter 2 of the thesis, in most front tracking techniques the interface is located by balancing fluxes between the frozen and unfrozen sections in the tissue. For a tissue freezing problem the governing equation for the solid phase in two dimensions is;

$$\frac{\partial T_s}{\partial t} = \alpha_s \left(\frac{\partial^2 T_s}{\partial x^2} + \frac{\partial^2 T_s}{\partial y^2} \right) \tag{1}$$

diffusion in the unfrozen section is governed by the following equation;

$$\frac{\partial T_l}{\partial t} = \alpha_l \left(\frac{\partial^2 T_l}{\partial x^2} + \frac{\partial^2 T_l}{\partial y^2} \right) \tag{2}$$

and the interface continuity equation is given by (Shyy *et al*, 1996);

$$\frac{\partial s}{\partial t} = \frac{1}{\rho L} \left(-k_l \frac{\partial T_l}{\partial n} + k_s \frac{\partial T_s}{\partial n} \right) \tag{3}$$

It is evident from Eqn (3) that if the entire latent heat (335 KJ/Kg) is released instantaneously at a phase change temperature, then the front velocity would be much lower than the case when the same amount of latent heat is released in fractions over a range of temperatures. This would consecutively increase the cooling rates in the tissue; as ice formation rate would be much higher than previously discussed.

The objective of this Chapter is to present a two dimensional diffusion model with temperature dependent thermophysical properties for the frozen section, as well as the effect of temperature dependence of the latent heat, and numerical simulations to predict cooling rates in tissues irradiated by lasers and exposed immediately to liquid nitrogen temperatures.

4.2 Physical model and governing equations

As stated earlier, to prevent damaging effects associated with traditional freezing it becomes essential that cooling rates attained in any section of the tissue be of the order of 8,000-10,000 ^{o}C/min. Water being the main constituent of any biological system, the thermophysical properties of the tissue being frozen can be approximated to be that of water (Devireddy *et al*, 2002 (c)). To accurately capture the temperature profiles within the tissue we model it as a two dimensional rectangular structure in cartesian coordinates.

The computational domain and expected freeze front propagation with the initial and boundary conditions is illustrated in Fig 4.1 where a rectangular section of the tissue t mm thick and w mm wide is irradiated by laser pulse and brought in contact with the cryogenic fluid (liquid nitrogen). Essentially in the light-tissue interactions only the light absorbed by water is converted to heat energy. The absorption length α_l^{-1} can be related to the laser fluence F_l as $F_l = E_l \alpha_l^{-1}$ where E_l is the required laser beam energy given by the expression $E_l = EV$; E being the energy density for a given transformation volume

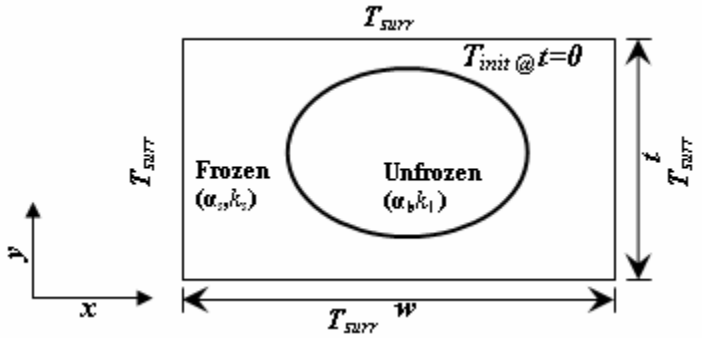

Fig 4.1 Two dimensional rectangular geometry of the freezing tissue section with initial and boundary conditions. Freeze front propagates within the tissue and separates the frozen and unfrozen regions of the section.

transformation V. The other important parameters that need to be chosen in light tissue interaction are the pulse width (t_p), reflectivity (R) and the absorption coefficients (α_l). Pulse width can be related to the characteristic length L_{tr} and thermal diffusivity D as $t_p < L_{tr}^2/4D$. For water the typical values of reflectivity and the absorption coefficients are ~0.019 and ~50μm respectively (Cammarata and Waulet, 1999; Jacques and Prahl, 1987). The intensity of the laser is given by;

$$I_o = \frac{P}{A}\left[\frac{w}{m^2}\right];\ A = \frac{\pi d_b^{\,2}}{4}[m^2]; \tag{4}$$

$$P = \frac{E}{t_p}[W] \tag{5}$$

where P is the power due to a pulse width t_p and A is the spot size (Cammarata and Waulet, 1999). These laser parameters (eg: wavelength, pulse width, spot size etc.) can be decided on the basis of energy that needs to be deposited to achieve the intended cooling rates.

The effect of microscale heat transfer on macroscale has been investigated earlier and suggests that the macroscale results are not affected by the microscale phenomena (Devireddy *et al*, 2002 (c)). Thus the conservation of energy equation for this system in the dimensional form is (Devireddy *et al*, 2002; Carslaw and Jaeger, 1959);

$$\frac{\partial}{\partial x}(k_s(T)\frac{\partial T_s}{\partial x}) + \frac{\partial}{\partial y}(k_s(T)\frac{\partial T_s}{\partial y}) + \tilde{Q} = \rho_s c_s(T)\frac{\partial T_s}{\partial t}; \tag{6}$$

$$\frac{\partial}{\partial x}(k_l\frac{\partial T_l}{\partial x}) + \frac{\partial}{\partial y}(k_l\frac{\partial T_l}{\partial y}) + \tilde{Q} = \rho_l c_l\frac{\partial T_l}{\partial t}; \tag{7}$$

Eqn. (6) and Eqn. (7) are the governing equations applicable for the frozen and unfrozen regions of the computational domain respectively. k, c, ρ are the thermal conductivity specific heat and the density of the tissue, *'s'* as subscript indicates the solid or the frozen region and '*l*' the liquid or the unfrozen region within the tissue. To accurately capture the cooling rates in the tissue section the thermophysical properties for the frozen section are taken to be temperature dependent (as shown in Table 4.1). Note that $\tilde{Q}$ represents the instantaneous heat input from the laser pulse. In the thermal diffusion model governed by Eqn. (6) and Eqn. (7) the incident laser beam profile is assumed to be "top hat" type, and the beam intensity decays exponentially as it propagates within the medium according to the Beer's law, as $\tilde{Q} = I_o(1-R)\exp(-\alpha_l x)$; where I_o is the

unattenuated intensity of the laser at the exit ($x=0$), R is the reflectivity of the sample and α_l is the absorption coefficient as mentioned earlier (Cammarata and Waulet, 1999). Eqn. (6) and Eqn. (7) are coupled using the apparent heat capacity method where the specific heat at the phase change interface, a common region shared by the frozen and unfrozen section, is approximated by Eqn. (8) (Alexiades and Solomon, 1984).

$$c_p = \frac{L_{ht}(T)}{\Delta T} \tag{8}$$

In the numerical model latent heat ($L_{ht}(T)$) is assumed to be released at temperatures ranging between -0.53 ^{o}C and -20 ^{o}C. The smoothening function ΔT used was 0.01 ^{o}C. The choice of this particular value for ΔT was justified since it led to faster convergence

Table 4.1 Thermophysical properties used to solve the coupled Eqn. (6), Eqn. (7) and Eqn. (8) and the initial and boundary conditions Eqn. (10), Eqn. (11).

Thermophysical Constant	Value and units
k	0.6 W/m-K (unfrozen) $2.24+0.005975(273-T)^{1.156}$ W/m-K (Frozen)
C_p	4200 J/Kg-K (unfrozen) 7.16T+138 J/Kg-K (frozen)
ρ	999 Kg/m^3 (unfrozen) 921 Kg/m^3 (frozen)
L	335000 J/kg
T_{ph}	-0.53+273 K
T_{surr}	-164+273 K
T_{init}	37+273 K

of the numerical simulation. Similar observations were made in earlier studies which suggest that a lower value of the smoothening temperature might lead to erroneous numerical round off errors (Alexiades and Solomon, 1984). The functional form of the fraction of latent heat of fusion released is given by Eqn. (9) as,

$$f(T) = 1 - \frac{A}{T_{ph} - T + A}; \quad T<T_{ph} \tag{9}$$

where T_{ph} is -0.53 ^{o}C for isotonic solutions and "A" is a constant equal to 0.53 (Devireddy, 1999; Devireddy *et al* 2002 (b)). The latent heat of fusion for water at -0.53 ^{o}C is 335,000 J/kg and $f(T)$ is the fraction of this energy released between -0.53 ^{o}C and T ^{o}C.

Eqn. (6) and Eqn. (7) are transient second order differential equations for which the assumed initial and boundary conditions presented in Fig 1 are,

$$T(x, y) = T_{init} \,@\, t = 0; \tag{10}$$

$$T(0, y) = T_{surr};\ T(d, y) = T_{surr};\ T(x,0) = T_{surr};\ T(x, m) = T_{surr} \ @ \ \ t > 0 \tag{11}$$

Boundary conditions of first kind shown in Eqn. (11) are chosen inspite of the symmetry in geometry as it would allow us to determine an approximate value for the cooling rate at the tissue center which should experience the least cooling rate. T_{init} and T_{surr} are the initial temperature (24 ^{o}C) and cryogenic fluid (-164 ^{o}C) temperature respectively.

4.3 Numerical algorithm and grid visualization

The coupled Eqns. (6)-(8) are solved on a fixed grid by a control volume based approach and using an alternating direction implicit technique, which is a second order accurate time stepping scheme, ideal for transient analysis (Patankar, 1980; Chung, 2002). The left hand terms in Eqn. (6) and Eqn. (7) were discretized using a second order accurate difference scheme and the non-linear temperature dependent thermophysical properties were resolved using the following iterative technique (Patankar, 1980).

1. Start with a guess or estimate for the values of temperature at all grid points (Initial tissue temperature).

2. From these guessed temperature fields calculate the tentative values of the coefficients in the discretization equations.
3. Solve the nominally linear set of algebraic equations to get new values of temperature fields.
4. Return to step 2 and repeat the process until further iterations cease to produce any significant changes in the predicted values of temperature.

To accurately account for the non-linear temperature dependence in the governing equations as well as the coupling equation, a higher convergence of 10^{-6} was chosen while iterating within the same temporal regime. Once the convergence is achieved the new temperature fields are updated and the solution is progressed to the next time step.

To optimize the computational time a 1051 by 1051 grid stencil is chosen so as to get acceptable grid resolution. As expected a finer spatial resolution of 2102 by 2102 was found to increase the computational time by 100% whereas the thermal history changed only by ± 0.05%. As an iterative scheme was used to resolve the intrinsic non-linearity an optimal value of time stepping of 0.1 sec was chosen. Again a finer temporal resolution of 0.01 sec effects the predicted thermal history only marginally (<0.001%). Due to the pulsed nature of the incident radiation the parameter $\tilde{Q}$ in Eqn. (6) and Eqn. (7) acts as an instantaneous source term and as such is applied at the second time step (at t=0.1sec). The source term obeys the Beer's law and is immediately forced to go to zero in the subsequent computations to mimic instantaneous laser irradiation. This is achieved using a Dirac delta formulation in the governing equation which forces the source term to zero for all subsequent temporal marches.

4.4 Numerical results

Heat source in our model is a pulsed Nd:YAG laser capable of delivering 360mJ of energy per pulse with a pulse width of ~6ns. Based on these parameters and the need to achieve cooling rates of ~10,000 ^{o}C/min throughout the tissue section a preliminary study

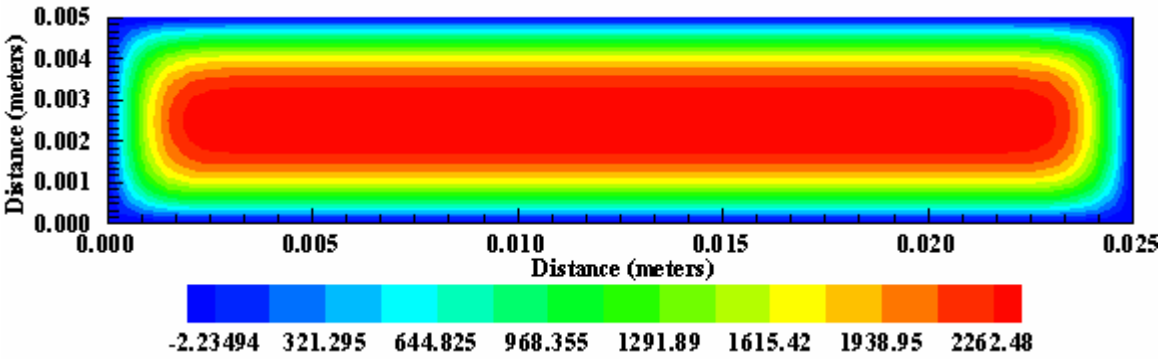

Fig 4.2A Temperature profiles within the tissue irradiated by an ultra-short laser pulse from a Nd:YAG laser at time t=0.1 sec, the average tissue temperature is about ~2000 ^{o}C.

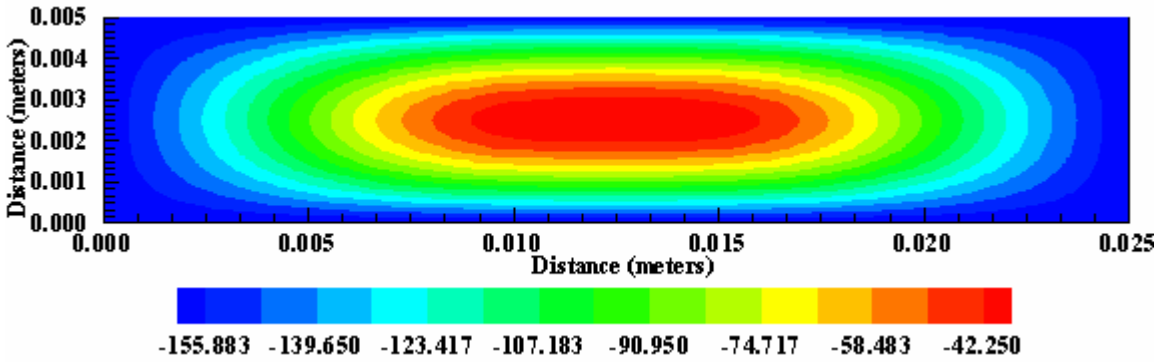

Fig 4.2B Temperature distribution within the tissue at time t=2.8 sec when every point within the tissue is ≤ ~ -140 ^{o}C.

determined that the maximum thickness and width for tissue as 5mm and 25mm respectively. To verify our numerical model it was compared with the standard analytical solution for the same dimensions in the case of constant thermophysical properties (Alexiades and Solomon, 1984). The model results differed from the analytical solution by ~0.6% (data not shown, in the interest of brevity) thus validating our model. The temperature distribution within the tissue at 0.1 sec, when irradiated by a pulsed laser and dipped in liquid nitrogen, is presented in Fig 4.2A. The maximum temperature that the

tissue reaches upon the diffusion of laser flux is about 2400 ^{o}C. Fig 4.2B indicates the predicted temperature profiles at 2.8 sec due to cooling caused by the cryogenic fluid in the laser heated tissue. As suggested by the results almost the entire tissue experiences temperatures below -100 ^{o}C. To further analyze the cooling rates in the tissue the isocooling rate contours and the thermal history at the center of the tissue are presented in

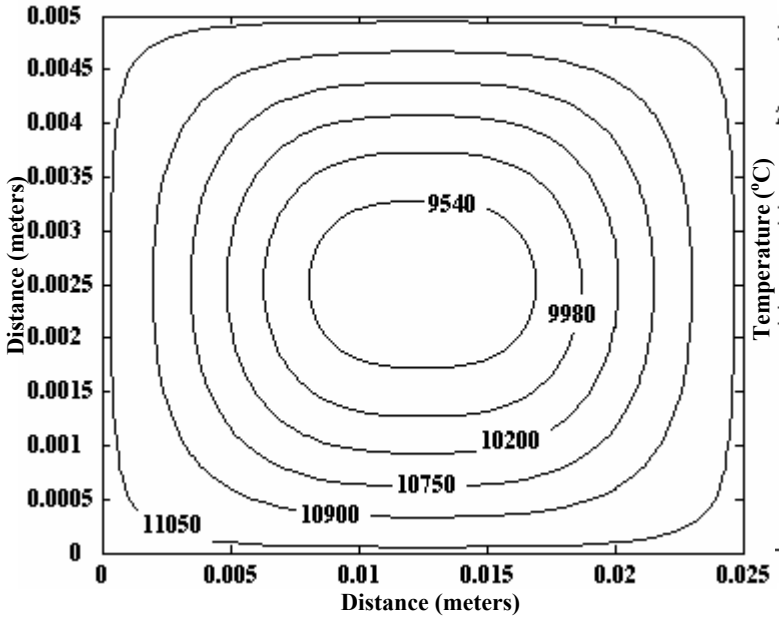

Fig 4.3A Model predicted iso-cooling rate contours for the case when the laser irradiated tissue section is dipped in cryogenic fluid. Cooling rate at the tissue center which experiences the least cooling rate is ~ 9540 ^{o}C/min.

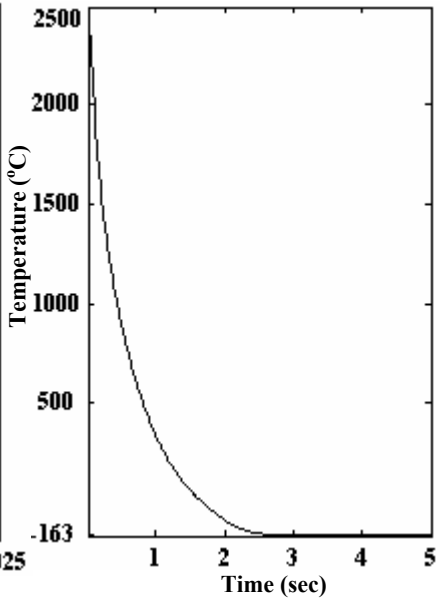

Fig 4.3B Thermal history at the tissue center suggests that it takes less than 3 secs for the tissue center to reach a temperature below -140 ^{o}C.

Fig 4.3A and Fig 4.3B respectively. It is evident that the predicted isocooling rates of ~11,000 ^{o}C/min at a location very close to the surface of the tissue and ~9,500 ^{o}C/min at the tissue center, measured between -0.53 ^{o}C and -140 ^{o}C, are high enough to achieve the desirable glass transition in freezing tissues and thus inhibiting the formation of extremely harmful intracellular ice crystals (Fahy, 1984). By letting $\tilde{Q}$=0 in our model we evaluated the cooling rates experienced by the tissue when dipped directly in liquid

nitrogen. Fig 4.4A and Fig 4.4B presents the predicted temperature distribution within the same tissue initially at 24 ^{o}C when brought in contact with cryogenic fluid at -164 ^{o}C,

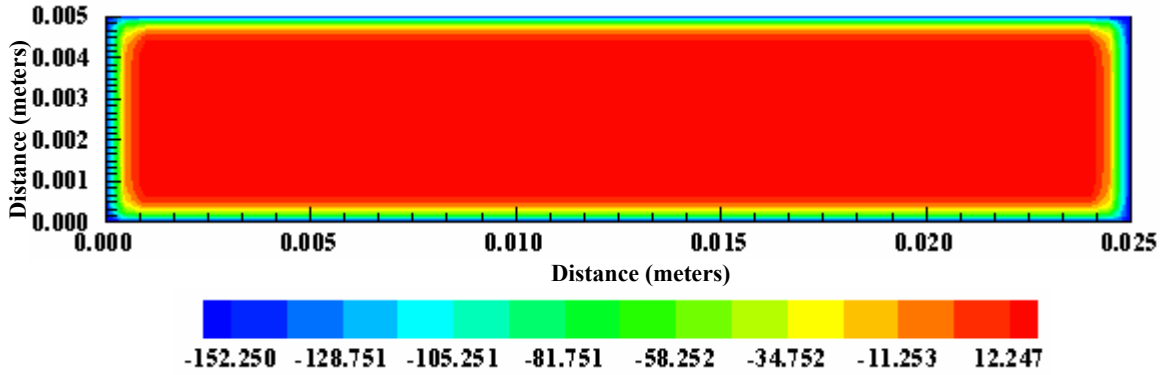

Fig 4.4A Temperature distribution within the tissue initially at 24 ^{o}C dipped in liquid nitrogen at -164 ^{o}C after dimensional time t=0.1 sec. Note that although the surface of the tissue almost immediately reaches the cryogenic fluid temperature and has the highest cooling rate associated with it, the center of the tissue is still at ~ 12.25 ^{o}C and experiences the least cooling rate.

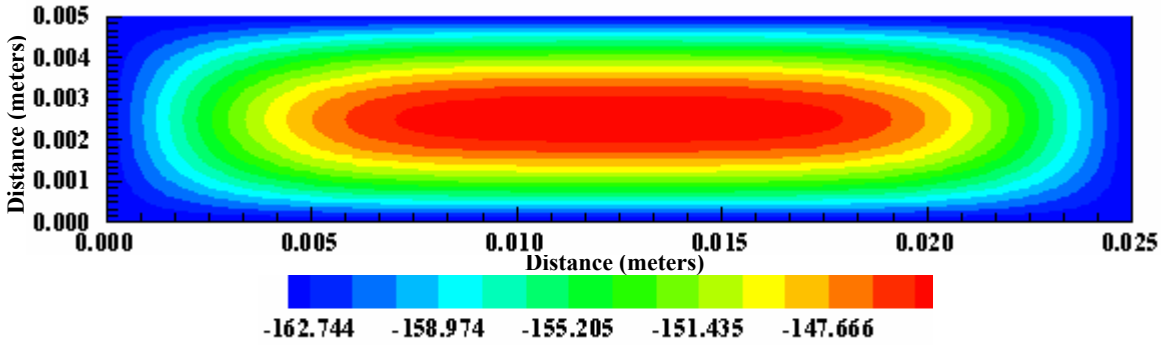

Fig 4.4B Temperature profiles within the tissue after dimensional time t=39.5 sec, at which every point within the tissue is $\leq \sim$ -120 ^{o}C.

corresponding to 0.1sec and 39.5sec respectively. Note the longer time it takes for the center of the tissue to reach -100 ^{o}C. The isocooling rate contours in Fig 4.5A and the thermal history at the center of the tissue in Fig 4.5B show that the maximum cooling rate is ~ 450 ^{o}C/min at a location very close to the surface of the tissue and the minimum cooling rate is ~240 ^{o}C/min at the center of the tissue measured between -0.53 ^{o}C and -140 ^{o}C. The simulation results indicate that cooling rates in the case of laser heated tissue dipped in liquid nitrogen are almost thirty times of those achievable when the same tissue is dipped directly into cryogenic fluid.

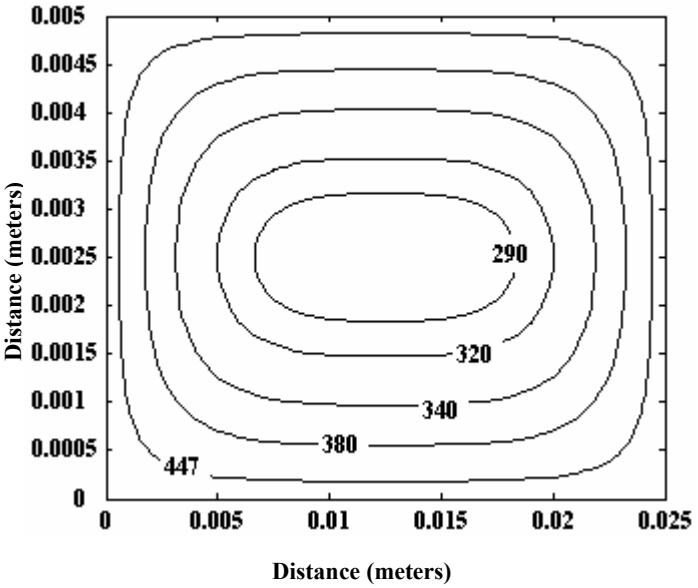

Fig 4.5A Model predicted isocooling rate contours in the tissue section initially at room temperature of 24 ^{o}C, in contact with the cryogenic fluid temperature of -164 ^{o}C. As expected the tissue surface experiences the maximum cooling rate of ~ 450 ^{o}C/min and the center experiences the least cooling rate of ~290 ^{o}C/min.

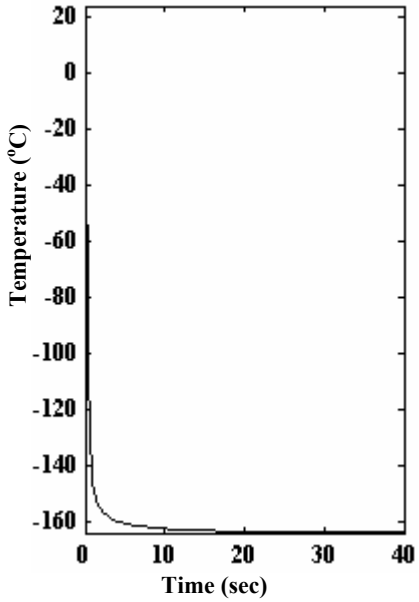

Fig 4.5B Thermal history at the tissue center suggests a location with the least cooling rate. Note that below the temperature of ~-147 ^{o}C the thermal history curve has a zero slope.

4.5 Conclusion

Temperature dependent latent heat has an intense effect on the cooling rates experienced in biological systems. It is seen that for finite sized tissue sections simulated as isotonic solutions the cooling rates experienced is twenty to thirty times greater than the case discussed earlier when the latent heat (335 KJ/Kg) was assumed to be released at -0.53 ^{o}C. Again for the case of the laser heated tissue dipped in liquid nitrogen the temperature dependence of latent heat augments in reducing the high temperature damage caused in the tissue section. The tissue stays at higher temperatures for a much shorter time than the case discussed earlier in Chapter 3.

Chapter 5

Average Thermal Damage Parameter and Its Effect on Viability of the Current Protocol

5.1 Introduction

As stated in the introduction, the purpose of our study was to investigate the effect of laser heating coupled with cryogenic temperatures to increase the thermal gradient (and consequently the cooling rates) experienced by tissues. In light-tissue interactions, only the absorbed light is used to generate heat within the tissue. Typically the incident irradiation is either absorbed by the water in the tissue or by hemoglobin in the blood or by melanin in the skin and is converted into heat (Cammarata and Wautelet, 1999). However, as shown in Fig 5.1 which is the thermal history as obtained from the one dimensional model of the laser tissue interaction (described in Chapter 3), a significant

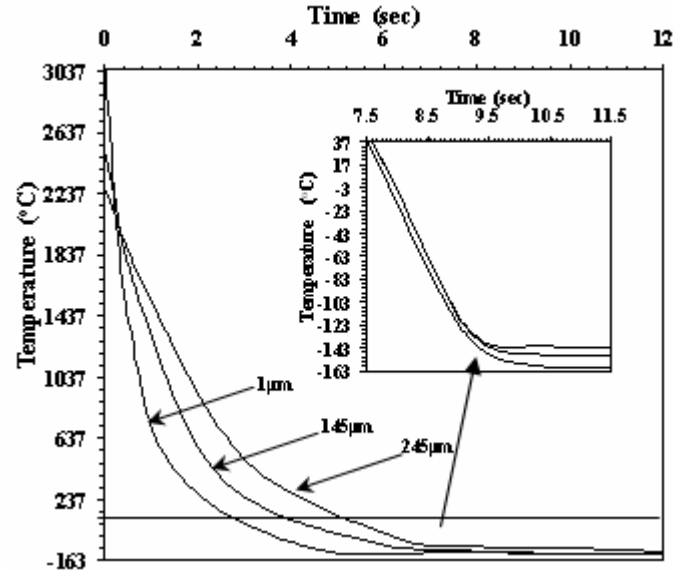

Fig 5.1 Thermal history at three different locations within the tissue section after it is exposed to laser irradiance of wavelength 488nm, beam diameter 2mm and pulse duration of 2 ns under cryogenic temperatures

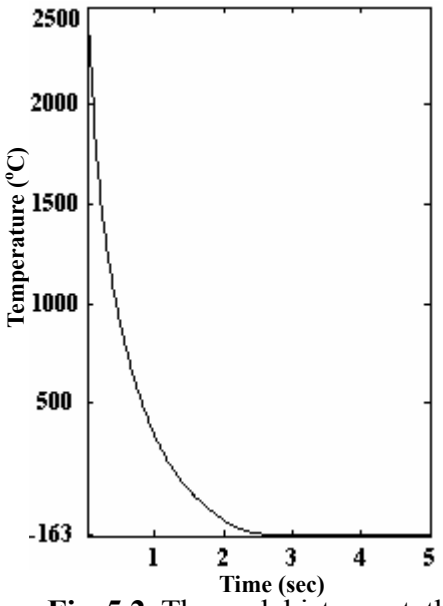

Fig 5.2 Thermal history at the tissue center suggests that it takes less than 3 secs for the tissue center to reach a temperature below -140 ^{o}C.

portion of the tissue section experiences very high residence time (~6 secs) at very high temperatures (>100 ˚C). Fig 5.2 is the thermal history at the laser heated tissue center as discussed in the two dimensional computational model incorporating the isotonic solution behavior of the tissue (Chapter 4). As this location is the farthest from the surrounding cryogenic fluid it is expected that the tissue center experiences the least cooling rates. It is evident from Fig 5.1 and Fig 5.2 that high temperatures will clearly damage the tissue via hyperthermic injury and tissue ablation (Cammarata and Wautelet, 1999; Walsh, 1995).

5.2 Average thermal damage parameter

In pulsed laser heating when the energy deposition occurs rapidly, water does not undergo a phase change at 100 ^{o}C with an immediate volume expansion, but rather the energy is deposited approximately isovolumetrically and the water temperature and pressure rise rapidly leading to an explosive ablation (Walsh, 1995). This rate process thermal damage can be quantified using the Arrhenius rate equation given by;

$$\Omega(r,t) = A\int_{0}^{t} \exp\left(-\frac{\Delta E}{RT(r,t)}\right)dt \qquad (1)$$

The high temperature thermal damage needs to be mitigated before the procedure described in the present study can be considered as a viable candidate for vitrifying tissue sections or for experimental validation. Fortunately, most cryopreservation/vitrification protocols utilize chemicals ranging in concentrations from 0.5 to 6 moles. In the presence of these chemicals the cooling rates needed to vitrify tissue sections are reduced to ~5000 to ~1000 ^{o}C/min (Fahy, 1998). The lower cooling rates needed to vitrify the

tissue section in the presence of chemicals will clearly reduce the high temperature

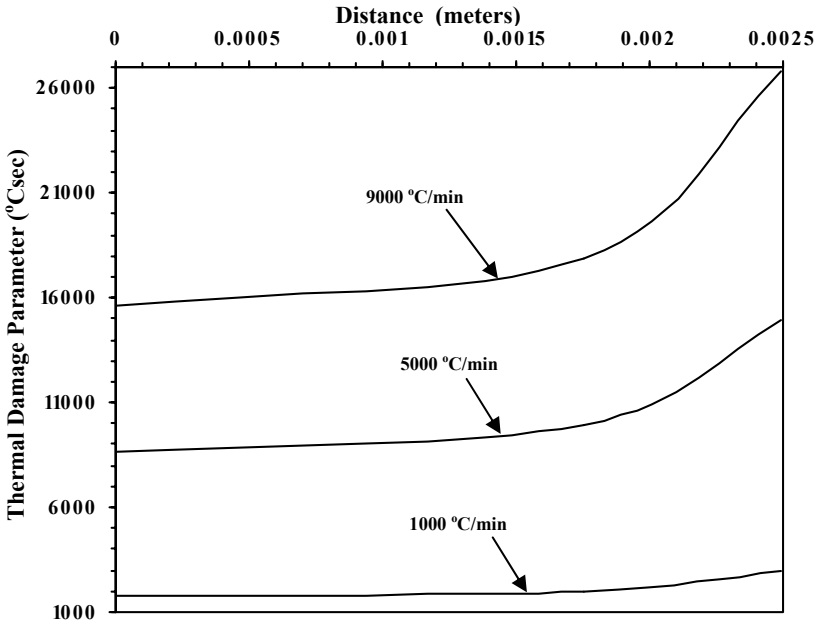

Fig 5.3 Measure of thermal damage with three different cooling rates.

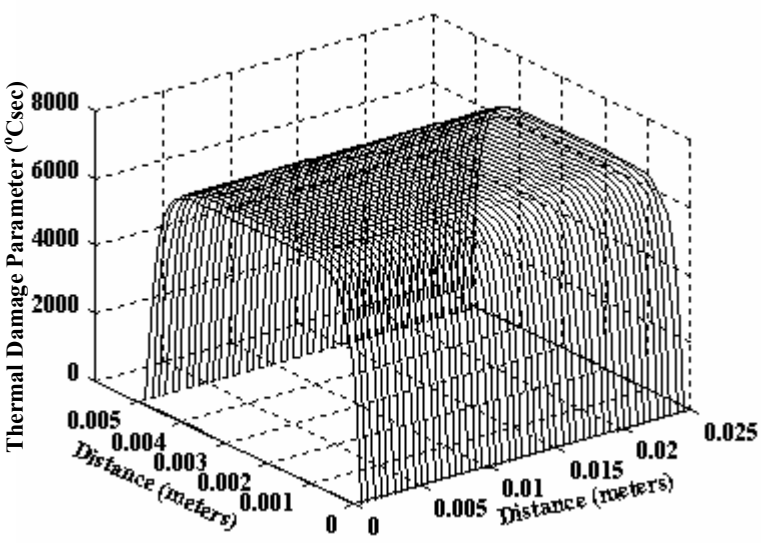

Fig 5.4 Average thermal damage parameter in the laser irradiated tissue measured as the product of maximum temperature at any given location and the time it takes for the tissue to reach -140 °C.

damage accumulated in the tissue (due to the fact that the thermal gradient necessary to achieve these slower cooling rates will be lower than that shown in Fig 5.1 and Fig 5.2). To further investigate this effect, we defined a "high temperature damage parameter" as

the product of the residence time (or the time the tissue section experiences temperatures greater than 40 ˚C) and the maximum temperature experienced by the tissue (and is shown in Fig 5.3 and Fig 5.4). Fig 5.4 which corresponds to the two dimensional model (Chapter 3) clearly indicates that the thermal damage parameter at the center of the tissue is much higher than the surface of the tissue which could cause ablation at the tissue center (Walsh, 1995). This crude approximation of thermal damage, it is anticipated, will serve as a parameter to compare the relative high temperature damage associated with laser heating necessary to achieve vitrification. As expected, as the cooling rate required to vitrify the tissue is decreased the "high temperature damage parameter" is reduced as well (Fig 5.3). Thus, raising the hope that a large tissue section (0.5 cm thick) loaded with chemicals, irradiated with pulsed lasers and immediately exposed to liquid nitrogen temperatures will not only vitrify but also survive the exposure to high temperatures.

Chapter 6

Experimental Validation of the Novel Cryopreservation Protocol

6.1 Motivation

Alternate cryopreservation protocols for preserving dimensionally large tissue sections could be a long term solution to transplantation crisis. Vitrified tissue samples form thermodynamically, structurally as well as physically stable ice and can be rethawed back to their original state, preserving the biophysical parameters of the living system. As achieving high cooling rates uniformly in tissue sections has been an engineering challenge, a novel cryopreservation technique has been presented in this study where the thermal gradient existing between the laser heated tissue section and the surrounding cryogenic fluid forces the cooling rates to ~10,000 ^{o}C/min. A one dimensional computational model to predict cooling rates in 5mm thick tissue section was discussed in Chapter 3. It was inferred from the numerical results that cooling rates of the order of ~10,000 ^{o}C/min could be achieved when laser heated tissue sections are exposed to liquid nitrogen temperatures. The cooling rates numerically predicted during freezing of two dimensional isotonic solutions and a preliminary analysis of the thermal damage parameters support the claims of achieving cooling rates in excess of 10,000 ^{o}C/min throughout the tissue slice. The current Chapter presents preliminary experimental results for a variety of cryobiologically relevant solutions and using adipose tissue derived adult stem cells.

6.2 Experimental methods

The purpose of our preliminary experiments was qualitative visualization of the nature of ice formed at high cooling rates for dilute aqueous solutions with and without commonly used CPA's. The laser used in our experimental approach was a Q-Switched Quanta-Ray DCR-3 laser (Nd:YAG Laser) operating in the second harmonic at 532 nm. The laser irradiance consisted of pulses with a pulse width of ~5-7 nsec and a pulse energy stability of 3%. The pulse energy at a pulse repetition rate of 1Hz was about 360mJ and the peak power delivered was about 60 MW (Quanta-Ray, DCR-3 and DCR-4 Pulsed ND: YAG Laser shown in Fig 6.1). To mimic the geometry and constant temperature boundary conditions used in our numerical model the samples were held in a

Fig 6.1 Experimental set up consisting of Quanta-Ray DCR-3 laser and liquid nitrogen storage tank.

Fig 6.2 Copper model rectangular box for holding the samples.

copper (sheet thickness 0.5mm) molded rectangular box 5mm thick, 25mm wide and 15mm long as shown in Fig 6.2. A silicone based sealant (archer silicone rubber sealer) was used to make the samples airtight. To realize the first kind boundary conditions used in our numerical model, the rectangular box is irradiated by a short laser pulse and

immediately immersed into a liquid nitrogen tank. The samples used were primarily water and physiologically isotonic phosphate buffered saline solutions (PBS) loaded with various concentrations of CPA's.

Opaque crystalline ice formed due to nucleation at lower cooling rates when the copper box filled with water is directly dipped into liquid nitrogen is shown in Fig 6.3.

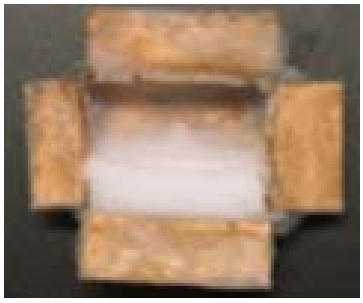

Fig 6.3 Water when dipped in LN2

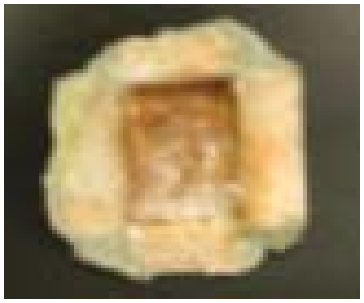

Fig 6.4 5% Glycerol and water irradiated and dipped in LN2

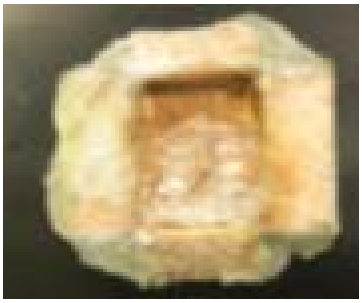

Fig 6.5 Transition from glassy to crystalline state **Fig 6.4**

Visual inspection clearly showed that the copper box base is invisible when seen through the crystalline ice (Fig 6.3). Fig 6.4 shows picture of water with 5% glycerol irradiated by laser and immediately dipped in liquid nitrogen (note that 5% glycerol is typical of most cryopreservation protocols and biological systems do not exhibit any deleterious toxicity at this concentration). Visual inspection indicates formation of transparent (possibly glassy) ice as the bottom of the copper box is clearly observable. The transformation of the transparent ice to opaque or crystalline ice after exposure to room temperature was also observed (Fig 6.5) and is encouraging in that it suggests that the transparent ice formed was not due to photo bleaching or laser induced chemical reactions (Fowler and Toner, 1997). However further corroboration of the formation of glassy ice needs to be validated using polarization microscopy and differential thermal analysis to detect the release of latent heat. At higher concentration of CPA's when 10%

glycerol is added to water, irradiated with an ultra short pulse and dipped in liquid nitrogen is shown in Fig 6.6. The transition from a transparent to crystalline state is seen in Fig 6.7. For physiologically isotonic solution PBS loaded with 10% glycerol the amorphous crystal free ice is presented in Fig 6.8. As predicted by the two dimensional numerical model which took isotonic solution properties in account, Fig 6.8 clearly

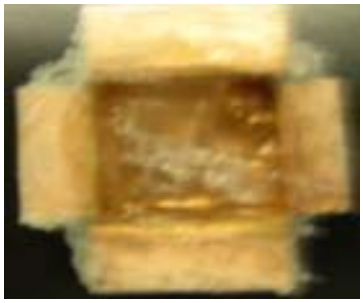

Fig 6.6 10% glycerol in water irradiated and dipped in LN2

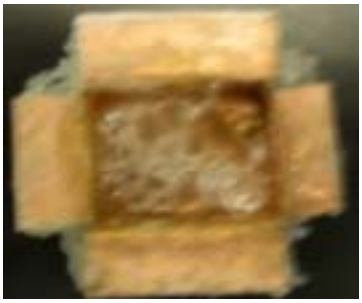

Fig 6.7 Transition from glassy to crystalline state for **Fig 6. 6**

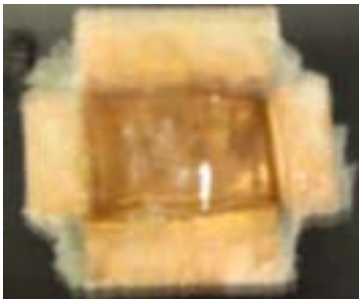

Fig 6.8 10% glycerol in PBS irradiated and dipped in LN2.

Fig 6.9 Transition from glassy to crystalline state for **Fig 6.8**

shows the formation of amorphous ice. The transition from transparent to crystalline state is seen in Fig 6.9. Further results on glassy states and transition from glassy to crystalline state for various CPA concentrations in water and PBS can be seen in Fig 6.10-6.12.

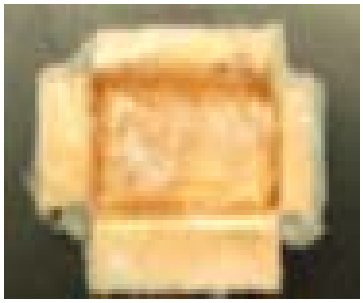

Fig 6.10 20% glycerol in PBS irradiated and dipped in LN2.

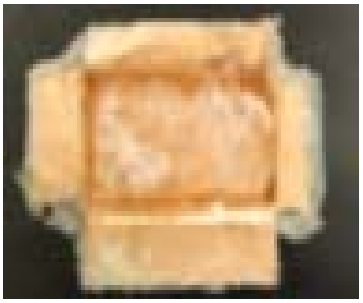

Fig 6.11 Transition from glassy to crystalline state for **Fig 6.10**

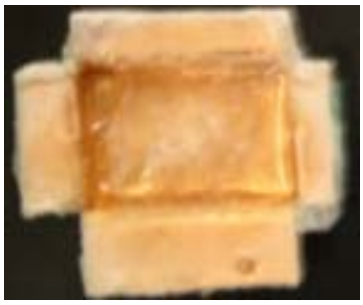

Fig 6.12 20% glycerol in water irradiated and dipped in LN2.

To further study the efficacy of the current protocol, freezing experiments were conducted on adipose tissue derived adult stem cells in phosphate buffered saline solution with 10% glycerol (Aust *et al*, 2004). The average cell survival at the beginning of the experiment was 98.4% ± 1%; cell viability was assessed using membrane excluded fluorescent dyes (Garner and Johnson, 1995; Devireddy *et al*, 2000). As shown in Fig 6.13, when the cells were enclosed in a copper box of 0.5cm x 2.5cm (imitating our earlier numerical results shown in Chapter 3 and Chapter 4), laser irradiated and exposed to liquid nitrogen (cooling rate of ~ 10,295 ^{o}C/min) had a viability of 67% ± 10%. Similarly, when cells were exposed directly to liquid nitrogen (note that as before the cell

suspension was enclosed and sealed in copper box), the viability reduced significantly to 9% ± 10% (this corresponds to a cooling rate of ~370 ^{o}C/min). This result was very encouraging and demonstrated the feasibility of using lasers and liquid nitrogen to

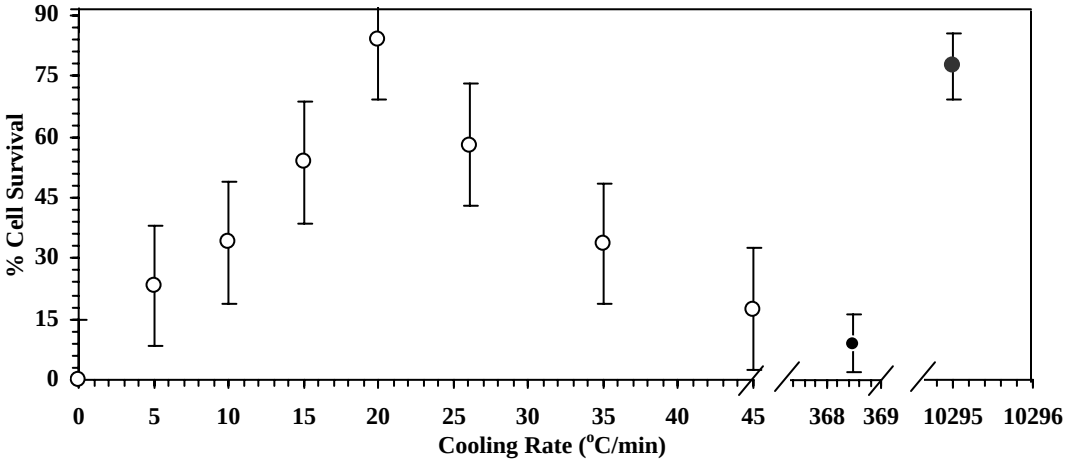

Fig 6.13 Percentage cell survival at various cooling rates.

successfully preserve the viability of frozen-thawed adult stem cells. In the interest of completeness, additional experiments at a range of cooling rates (from 1 ^{o}C/min to 45 ^{o}C/min) were also performed using a controlled rate freezer, CRF (PLANER, TS Scientific, Perkasie, PA; Devireddy *et al*, 2003; Neidert *et al*, 2004). As shown in Fig 6.13, the cell survival vs. cooling rate has a characteristic inverse U curve shape, denoting the loss of cell viability at low cooling rates (<20 ^{o}C/min) and cell viability at high cooling rates (>20 ^{o}C/min) due to solution effects and the formation of damaging intracellular ice formation. The highest post cell viability was for a cooling rate of 20 ^{o}C/min and was found to be 85% ± 5%. Although, this value is somewhat higher than the one obtained when the cells were laser irradiated and immediately exposed to liquid nitrogen, it should be noted that in the controlled rate freezer samples were cooled only to -30 ^{o}C (i.e. it is possible that cooling these cells to ~-160 ^{o}C will diminish the cell

viability). Additionally, no effort was made to understand or optimize the thawing rates (an uniformly high thawing rate of ~200 ^{o}C/min was employed). It should be noted that the preliminary results are very encouraging and suggest that "Lasers and Liquid Nitrogen" could form the basis of a novel and viable low temperature storage process for tissue sections.

6.3 Conclusions

An alternative cryopreservation protocol to achieve high cooling rates to obtain vitrified samples has been suggested. Numerical simulations and experimental results indicate the possibility of heating biological tissues to extremely high temperatures, by carefully choosing an energy deposition source. Cooling rates of ~10,000 ^{o}C/min can then be achieved throughout the tissue section due to the thermal gradient existing between the tissue at the elevated temperature, and the surrounding cryogenic fluid. Preliminary experimental results indicate that vitrified samples could be achieved using this protocol though further studies are clearly needed. Preliminary investigations on the post thaw survival of adipose tissue derived adult stem cells using the proposed new protocol show some promise.

Chapter 7

Conclusion and Future Improvements

7.1 Conclusion

The current study focused on suggesting an alternative cryopreservation protocol to vitrify biological tissues by freezing them at cooling rates of ~10,000 ^{o}C/min. The one dimensional numerical model for 5mm thick tissue section and assuming temperature dependent thermophysical properties for the frozen section and phase change at a fixed temperature of -0.53 ^{o}C clearly showed that the freezing tissue could be vitrified. Results from an extended two dimensional model taking into account the isotonic behavior of the cell water in the tissue (5mm thick and 25mm wide) suggested that the cooling rates were twenty to thirty times higher than what could be achieved in the one dimensional mode. The thermal damage parameter for the two dimensional model clearly indicated that the ablation would be significantly reduced when experiments would be carried on actual samples. The experimental results on cryobiologically relevant solutions and adipose tissue derived adult stem cells show that by exposing laser heated solutions to cryogenic temperatures potential glassy states could be achieved. The survival results of the stem cell were encouraging in that it could effectively address the "Transplantation Crisis" if the suggested protocol could be optimized.

7.2 Future Improvements

Future improvements to optimize the suggested protocol should include the following:

1. Our model currently assumes that the thermal wave propagates at an infinite velocity within biomaterials. A refined numerical model should be developed based on non

Fourier heat conduction, which takes into account the thermal relaxation time within the biomaterials, to accurately predict the temperature distribution and cooling rates within biological systems (Deng and Liu, 2003).

2. When energy deposition occurs rapidly, water does not undergo a phase change at 100 ^{o}C with an immediate volume expansion, but rather the energy is deposited approximately isovolumetrically and the water temperature and pressure rise rapidly leading to an explosive ablation (Walsh, 1995). Our numerical model currently does not account for this phenomenon which needs to be incorporated in future modeling efforts.
3. Additional variables and unresolved issues include sensitivity of tissue cells to high temperature damage which might in turn effect the viability of the alternate cryopreservation protocol, effect of assuming a Gaussian beam intensity profile as well as shorter pulses, possible use of varying (and time dependent) laser energy deposition, possible ablative coatings to prevent tissue loss and the possibility of thermal stress and vascular damage that might result in the tissue during the heating and freezing process could be considered.
4. Future experiments should include Differential Thermal Analysis (DTA) and X-Ray Diffraction to study the nature of ice formed with and without laser irradiation in a variety of solutions to confirm or refute the formation of glassy ice visually obtained as part of this current study (Mazur, 1963; Chen *et al*, 1997).

References

Alexiades V, Solomon A D, *Mathematical Modeling of Melting and Freezing Processes*, Hemisphere Publishing Corporation, New York, (1993).

Aust L, Devlin B H, Foster S J, Halvorsen Y D C, Hicok K, Kloster A L, Laney Du T V, Sen A, Willingmyre D, Gimble J M, Cytotherapy: Recovery of human adipose derived adult stem cells from liposuction aspirates **6**, 7-14(2004).

Bischof J C, Rubinsky B, ASME Journal of Heat Transfer: Microscale heat and mass transfer of vascular and intracellular freezing in the liver **115**, 1029-1035 (1993).

Bischof J C, Ryan C M, Tompkins R G, ASAIO Journal: Ice formation in isolated human hepatocytes and human liver tissue **43**, 271-278 (1997).

Bourton P, Cryobiology: Comparison with the theory of kinetics and extent of ice crystallization and of the glass-forming tendency in aqueous cryoprotective solutions **23**, 88-102 (1986).

Cammarata F, Wautelet M, Physics Update: Medical lasers and laser-tissue interactions **34**, 156-161 (1999).

Carslaw H S, Jaeger J C, *Conduction of Heat in Solids*, Oxford University Press, Oxford, UK, (1959).

Chen C C, Herhold A B, Johnson C S, Alivisatos A P, Science: Size dependence of structural metastability in semiconductor nanocrystals **276**, 398-401 (1997).

Chung T J, *Computational Fluid Dynamics*, Cambridge University Press, New York, 141 (2002).

Day S H, Nicole-Griffith D A, Silva J M, Cryobiology: Cryopreservation of rat and human liver slices by rapid freezing **38**, 154-159 (1999).

Deng Z S, Liu J, 2003, Journal of Thermal Stresses: Non-Fourier heat conduction effect on prediction of temperature and thermal stress in skin cryopreservation **26**, 779-798 (2002).

Devireddy R V, Ph.D Dissertation: Measurement of freezing processes in biological systems, University of Minnesota, Minneapolis, MN (1999).

Devireddy R V, Swanlund D J, Roberts K P, Pryor J L, Bischof J C, Human Reproduction: The effect of extracellular ice and cryoprotective agents on the water permeability parameters on human sperm plasma membrane during freezing **15**, 1125-1135 (2000).

Devireddy R V, Olin T, Vincente W, Troedsson M H T, Bischof J C, Roberts K P, Biology of Reproduction: Cryopreservation of equine spermatozoa: Optimal cooling rates in the presence and absence of cryoprotective agents **66**, 222-231 (2002 (a)).

Devireddy R V, Leo J S, Lowengrub P H, Bischof J C, International Journal of Heat and Mass Transfer: Measurement and numerical analysis of freezing in solutions enclosed in small container **45**, 1915-1931 (2002 (b)).

Devireddy R V, Smith D J, Bischof J C, Journal of Heat Transfer: Effect of microscale mass transport and phase change on numerical prediction of freezing in biological tissues **124**, 365-374 (2002 (c)).

Devireddy R V, Neidert M R, Bischof J C, Tranquillo R T, Tissue Engineering: Cryopreservation of collagen-based tissue-equivalents - Part I: Effect of freezing in the absence of cryoprotective agents **9**, 1089-1100 (2003).

Diller K R, Cryobiology: Intracellular ice formation in glycerolized red cells **16**, 125-131 (1979).

Doremus R H, *Fracture of Glas:* in Glass Science*,* Wiley-Interscience, New York, 281-295 (1973).

Fahy G M, Hirsh A, *Organ Preservation, Basic and Applied Aspects* (Pegg D E, Jacobsen I A, Halasz N A, Eds.), MTP Press, Lancaster, 399-404 (1982).

Fahy G M, MacFarlane D R, Angell C A, Meryman H T, Cryobiology: Vitrification as an approach to cryopreservation **21**, 407-426 (1984).

Fahy G M, *Biological Effects of Vitrification and Devitrification: in The Biophysics of Organ Cryopreservation* (Pegg D E, Karow A M, Eds.), Plenum Press, New York (1987).

Fahy G M, Vitrification in: Low Temperature Biotechnology: Emerging Applications and Engineering Contributions (Diller K R, Eds.) **10**, New York, 113-146 (1988).

Fahy G M, Journal of Heat Transfer: Vitrification **98**, 113-146(1998).

Fowler A J, Toner M, Journal of Heat Transfer: Cryopreservation of cells using ultra-rapid freezing **37**, 179-183 (1997).

Gardner C M, Jacques S L, Welch A J, Lasers in Surgery and Medicine: Light transport in tissue: accurate expressions for one-dimensional fluence rate and escape function based upon Monte Carlo simulation **18**, 129-138 (1996).

Garner DL, Johnson LA, Biological Reproduction: Viability assessment of mammalian sperm using SYBRI4 and propidium iodide **53**, 276-284 (1995).

Hallburcker A, Mayer E, Johari G P, Journal of Physical Chemistry: Glass liquid transition and the enthalpy of devitrification of annealed vapor-deposited amorphous solid water. A comparison with hyperquenched glassy water **93**, 4986-4990 (1989).

Han B, Bischof J C, Cell Preservation Technology: Engineering challenges in tissue preservation **2,** 91-111 (2004).

Handa Y P, Klug D D, Journal of Physical Chemistry: Heat capacity and glass transition behavior of amorphous ice **92**, 3323-3325 (1988).

Hartmann U, Nunner B, Korber C, Cryobiology: Where should the cooling rate be determined in an extended freezing sample? **28**, 115-130 (1991).

Hayes L J, Diller K R, Journal of Energy Research Technology: Implementation of phase change in numerical models of heat transfer **105**, 431-435 (1983).

Hayes L J, Diller K R, Lee H S, Cryoletters: On the definition of an average cooling rate during cell freezing **5**, 97-110 (1984).

Hayes L J, Diller K R, Chang H, *A Robust Numerical Method For Latent Heat Release During Phase Change: in Numerical Methods in Heat Transfer* (Vafai K, Eds.) **62**, New York: ASME, 63-70 (1986).

Hayes L J, Diller K R, *Computational Methods For Analysis of Freezing Bulk Systems: in Low Temperature Biotechnology: Emerging Applications and Engineering Contributions* (Diller K R, Eds.) **62**, New York: ASME, 253-272 (1988).

Hayes L J, Diller K R, Chang H J, Lee H S, Cryobiology: Prediction of local cooling rates and cell survival during the freezing of a cylindrical specimen **25**, 67-82 (1988).

Ishiguro H, Rubinsky B, Cryobiology: Mechanical interaction between ice crystals and red blood cells during directional solidification **31**, 483-500 (1994).

Jacques S L, Prahl S A, Lasers in Surgery and Medicine: Modeling optical and thermal distributions in tissue during laser irradiation **6**, 494-503 (1987).

Johari G P, Hallburcker A, Mayer E, Journal of Physical Chemistry: Calorimetric study of pressure-amorphized cubic ice **94**, 1212-1214 (1990).

Jo J C, Shin W K, Choi C Y, Numerical Heat Transfer: Multidimensional phase change problems by the dual reciprocity boundary-element method **36**, 95-113 (1999).

Karlsson J O, Toner M, Cryopreservation: Principles of tissue engineering **2**, Academic Press, 243-256 (2000).

Kauzmann W, Chemical Reviews: The nature of the glassy state and the behaviors of liquids at low temperatures **43**, 219-256 (1948).

Levin R L, Cravalho E G, Huggins C G, Cryobiology: A membrane model describing the effect of temperature on water conductivity of erythrocyte membranes at subzero temperatures **13**, 415-429 (1976).

Lovelock J E, Biochimica et Biophysica Acta: Haemolysis of human red blood cells by freezing and thawing **10**, 414-426 (1953).

Lunardini V, *Heat Transfer in Cold Climates*, Van Nostrand Reinhold, New York, (1981).

Luyet B J, Biodynamica: The vitrification of organic colloids and of protoplasm **1**, 1-14 (1937).

MacFarlane D R, Forsyth M, *Devitrification and Recrystallization of Glass Forming Aqueous Solutions: in The Biophysics of Organ Preservation* (Pegg D E, Karow A M Jr. Eds.), Plenum Press, New York, 237-263 (1987).

McGrath J J, Cravalho E G, Huggins C E, Cryobiology: An experimental comparison of intracellular ice formation and freeze thaw survival of Hela S-3 cells **12**, 540-550 (1975).

McGrath J J, *Preservation of Biological Material by Freezing and Thawing: in Heat Transfer in Medicine and Biology* (Shitzer A, Eberhart R C, Eds.), Plenum Press, New York (1985).

Mayer E, Journal of Microscopy: Vitrification of pure liquid water **140**, 3-15 (1985).

Mazur P, Journal of General Physiology: Kinetics of water loss from cells at subzero temperatures and the likelihood of intracellular freezing **47**, 347-369 (1963).

Mazur P, *Physical and Chemical Basis of Injury: in Single Celled Micro-Organisms Subjected to Freezing and Thawing in Cryobiology* (Meryman H T, Eds.), Academic Press, London (1966).

Mazur P, Science: Cryobiology: The freezing of biological systems **168**, 939-949 (1970).

Mazur P, American Journal of Physiology: Freezing of living cells: Mechanisms and implications **247**, C125-C142 (1984).

Neidert M R, Devireddy R V, Tranquillo R T, Bischof J C, Tissue Engineering: Cryopreservation of collagen-based tissue-equivalents - Part II: Improved freezing in the presence of cryoprotective agents **10**, 23-32 (2004).

Ozisik M N, Heat Conduction, Wiley, New York, (1993).

Patankar S V, Numerical Heat Transfer and Fluid Flow, Hemisphere Publishing Corporation, New York, (1980).

Pearce J, Thomsen S, Optical thermal response of laser-irradiated tissue (Welch A J, Gemert M J C, Eds.) Plenum Press, New York, 561-603 (1995).

Rubinsky B, Cravahlo E G, International Journal of Heat and Mass Transfer: A finite element method for the solution of one-dimensional phase change problems **24**, 1987-1989 (1981).

Rubinsky B, Carvalho E G, Cryobiology: An analytical method to evaluate cooling rates during cryopreservation protocols for organs **21**, 303-320, (1984).

Spectra Physics, Quanta-Ray, DCR-3 and DCR-4 Pulsed ND: YAG Laser, Instruction Manual.

Thirumala S, Ferrer M S, Al-Jarrah A, Eilts B E, Paccamonti D L, Devireddy R V, Cryobiology: Cryopreservation of canine spermatozoa: theoretical prediction of optimum cooling rates in the presence and absence of cryoprotective agents **47**, 109-121 (2003).

Toner M, Cravalho E G, Journal of Applied Physics: Thermodynamics and kinetics of intracellular ice formation during freezing of biological cells **67**, 1582-1593 (1992).

Walsh J T, Pulsed laser angioplasty: *A Paradigm For Tissue Ablation, Optical-Thermal Response of Laser-Irradiated Tissue*, Plenum Press, New York, 865-901 (1995).

Whittingham D G, Leibo S P, Mazur P, Science: Survival of mouse embryos frozen to -196 and -269 ^{o}C **178**, 411-414 (1972).

Appendix: Letter of Permission

From: "Beth Darchi" <DarchiB@asme.org>
To: <dkandr1@paws.lsu.edu>
CC:
Subject: Re: Copyright letter
Date: Thu, 04 Nov 2004 16:27:03 -0500

My mistake, sorry. Please see enclosed.

Dear Mr. Kandra,
It is our pleasure to grant you permission to use Figures 1-8 and Table-1 from ASME paper "Numerical Investigation of a Novel Method to Vitrify Biological Tissues Using Pulsed Lasers and Cryogenic Temperatures", by D. Kandra, etal, paper number HT-FED2004-56197, Proceedings of HT-FED04, 2004 ASME Heat Transfer/Fluids Engineering Summer Conference, cited in your letter for inclusion in Chapter-3 in your Masters Thesis Dissertation electronically to the Graduate School and The Mechanical Engineering Department of the Louisiana State University.

As is customary, we ask that you ensure full acknowledgment of this material, the author(s), and ASME as original publisher on all printed copies being distributed.

Many thanks for your interest in ASME publications.

Sincerely,

Beth Darchi
Copyrights & Permissions
P: 212-591-7700
F: 212-591-7292
E: darchib@asme.org

Vita

Deepak Kandra was born in Cuddapah, Andhra Pradesh, India, in August 1979. He completed his high school studies and joined the undergraduate studies program in Mechanical Engineering at Bangalore University, Bangalore, India, in 1997. He finished his undergraduate studies in 2001. He joined Louisiana State University, Baton Rouge, to pursue his master's degree. He expects to receive the degree of Master of Science in Mechanical Engineering at the December 2004 commencement.